Charles University
Faculty of Science

Study programme: Genetics, Molecular Biology and Virology
Curriculum: Molecular Biology and Genetics of Eukaryotes

Bc. Michal Mitro

The impact of post-translational modifications on TRPC5 ion channel activation and modulation

Vliv posttranslačních modifikací na aktivaci a modulaci iontového kanálu TRPC5

Diploma thesis
Supervisor: Mgr. Lucie Zímová, Ph.D.

Prague 2023

Prohlášení:

Prohlašuji, že jsem závěrečnou práci zpracoval samostatně a že jsem uvedl všechny použité informační zdroje a literaturu. Tato práce ani její podstatná část nebyla předložena k získání jiného nebo stejného akademického titulu.

V Praze, 07.12.2023 …….

Bc. Michal Mitro

Poďakovanie:

Chcel by som úprimne poďakovať pani doktorke Lucii Zímovej za všetky rady, pomoc a cenné skúsenosti, ktoré mi poskytla počas vypracovania tejto diplomovej práce ako aj počas celého môjho štúdia na univerzite. Taktiež by som rád vyjadril veľkú vďaku pani docentke Vlachovej za prijatie do výskumnej skupiny TRP, odborný dohľad a najmä za možnosť získavať praktické skúsenosti a odborné vedomosti v oblasti biologického výskumu.

Abstract

Transient Receptor Potential Canonical 5 (TRPC5), a calcium-permeable ion channel, acts as a versatile receptor in sensory neurons, kidneys, and the brain, impacting inflammatory responses and various types of pain. While post-translational modifications influence TRPC5 gating and membrane trafficking, only a few have been described so far. The identification of phosphorylation sites was based on available high-throughput bioinformatics and mass spectrometry data. Subsequently, functional characterization of these sites was conducted by introducing phospho-mimicking aspartate or phospho-null alanine mutations using site-directed mutagenesis. Utilizing patch-clamp in whole-cell configuration, membrane currents evoked by voltage or agonist stimuli were examined. The results revealed that individual substitutions at the N-terminal S193 and S195 with aspartates significantly slowed the gating kinetics. Additionally, a gain-of-function phenotype was observed with S193A. Molecular dynamics simulations provided insight into how phosphorylation at S193 induces changes in interactions among neighboring subunits. Moreover, biotinylation experiments indicated that the alterations in the activity of the S193 mutations are not due to increased targeting of the channels to the plasma membrane. Taken together, these results functionally characterize a previously unrecognized site of putative phosphorylation which leads to the gating modulation of TRPC5 ion channel.

Key words: TRP, TRPC5 channel, post-translational modification, phosphorylation, ion channels, protein regulation, signal transduction

Abstrakt

Transientní receptorový potenciálový kanonický kanál 5 (TRPC5), propustný pro vápenaté ionty, se uplatňuje jako receptor v senzorických neuronech, ledvinách a mozku, kde ovlivňuje zánětlivé procesy a různé typy bolesti. Přestože se předpokládá, že posttranslační modifikace významně ovlivňují vrátkování TRPC5 a jeho transport na membránu, bylo těchto procesů dosud popsáno poměrně málo. Za využití dostupných bioinformatických databází a dat z hmotnostní spektrometrie byla identifikována v rámci předložené práce fosforylační místa. Následně byla provedena funkční charakterizace těchto míst zavedením aspartátových (napodobujících fosfát) nebo alaninových (neumožňujících vazbu fosfátu) mutací pomocí cílené mutageneze. Technikou terčíkového zámku v uspořádání snímání aktivity z celé buňky byly zkoumány membránové proudy vyvolané napětím nebo působením agonisty. Výsledky ukázaly, že individuální záměny S193 a S195 z N-koncové domény za aspartáty významně zpomalují kinetiku vrátkování. Kromě toho byl u S193A pozorován fenotyp zesílení funkce kanálu. Molekulárně dynamické simulace naznačily, že fosforylace S193 způsobuje změny v interakcích mezi sousedními podjednotkami. Biotinylace navíc potvrdila, že změny aktivity mutací S193 nejsou způsobeny zvýšeným transportem proteinu na plazmatickou membránu. Dohromady tyto výsledky identifikují doposud nepopsané místo možné fosforylace, jehož prostřednictvím dochází k významnému regulovaní funkce iontového kanálu TRPC5.

Klíčová slova: TRP, TRPC5 kanál, posttranslační modifikace, fosforylace, iontové kanály, regulace proteinů, přenos signálu

List of abbreviations

ARD	ankyrin repeats domain
CaM	calmodulin
CBII	second calmodulin-binding site
CBS	calcium-binding site
CIRB	calmodulin and IP_3 receptor binding
CNS	central nervous system
CryoEM	cryogenic electron microscopy
DAG	diacylglycerol
DSK	dual-specifity kinase
EA	englerin A
ECS	extracellular solution
EPSD	eukaryotic phosphorylation site database
ER	endoplasmic reticulum
ERK1	extracellular signal-regulated kinase 1
Gα	alpha subunit of G-protein
GFP	green fluorescent protein
GPCR	G-protein coupled receptor
HLH	helix-loop-helix
hTRPC5	human transient receptor potential channel subfamily C member 5
IP_3	inositol trisphosphate
MATra	magnetic assisted transfection
MD	molecular dynamics
MS	mass spectrometry
NHERF1/2	Na^+/H^+ exchanger regulatory factor 1/2
PBS	phosphate-buffered saline
PCR	polymerase chain reaction
PIP_2	phosphatidylinositol 4,5-bisphosphate
PKA	protein kinase A
PKC	protein kinase C
PLC	phospholipase C
PTM	post-translational modification
qPTM	quantitative post-translational modification

SEM	standard error of the mean
ThermoTRP	temperature-sensitive transient receptor potential channels
TK	tyrosine kinase
TMD	transmembrane domain
TRP	transient receptor potential
TRPA	transient receptor potential ankyrin
TRPC	transient receptor potential canonical
TRPC5	gene encoding transient receptor potential canonical 5
TRPML	transient receptor potential mucolipin
TRPP	transient receptor potential polycystin
TRPV	transient receptor potential vanilloid
VSLD	voltage sensing-like domain
WT	wild type

1 Introduction

The TRP (transient receptor potential) ion channel family is a diverse group of membrane proteins found in many organisms and involved in a wide range of physiological processes, including sensory perception, body temperature regulation, regulation of ion homeostasis, and cellular signaling (Venkatachalam & Montell, 2007). The TRP channel family is divided into six subfamilies (Figure 1) based on sequence homology: TRPC (canonical), TRPV (vanilloid), TRPM (melastatin), TRPA (ankyrin), TRPP (polycystin) and TRPML (mucolipin) (Nilius & Owsianik, 2010).

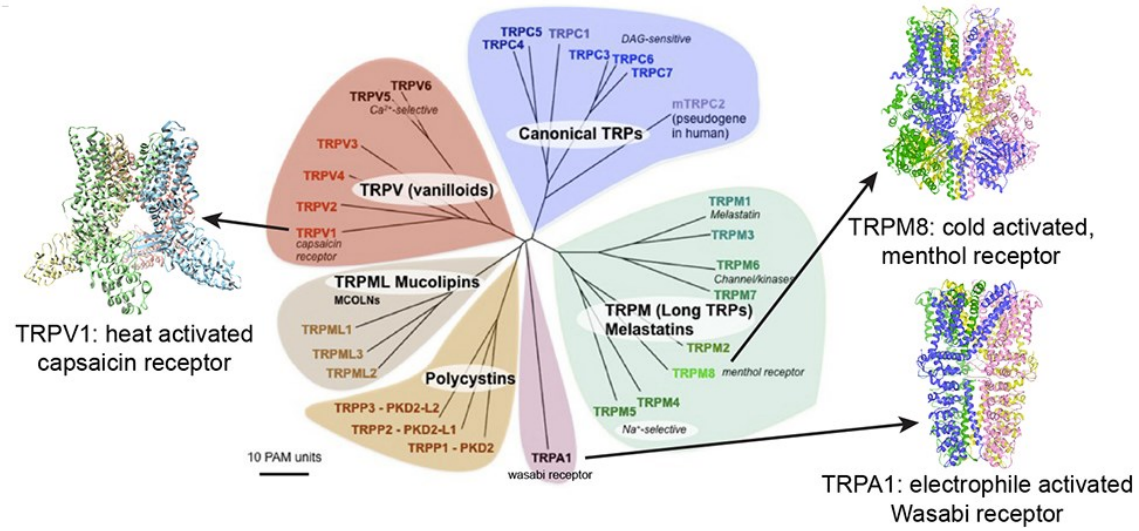

Figure 1: *Illustration showcasing the structures of TRPV1, TRPA1, and TRPM8, alongside the genetic tree of the TRP channel superfamily (adapted from Diver et al. 2022)*

TRP channels have been extensively studied over the past few decades, and numerous studies have been focused on their functions and the mechanisms underlying their activation. The ability of TRP channels to simultaneously respond and integrate various physical and chemical stimuli is known as polymodality (Nilius et al., 2007). The TRP channel family includes channels that are activated by heat and capsaicin (TRPV1), cold and menthol (TRPM8), mustard oil and cinnamaldehyde (TRPA1) (Venkatachalam & Montell, 2007). The activation of TRP receptors on the peripheral endings of nociceptive neurons initiates signal that travels through the spinal cord dorsal horn to the brain, leading to the experience of pain or acute discomfort (Julius, 2013). This pathway has gained significant attention due to its implications in the development of pain medications and therapies. Consequently, the 2021

Nobel Prize in Physiology or Medicine was awarded to David Julius and Arden Patapoutian for their discoveries in the identification and functional characterization of TRP channels, particularly TRPV1, TRPM8 and TRPA1, which are involved in pain and temperature sensation.

This thesis explores and functionally characterizes the phosphorylation sites of the TRPC5 channel attributed by mass spectrometry. The effects of phosphorylation on TRPC5 gating kinetics and functional expression were investigated using various methods, including electrophysiological techniques, site-directed mutagenesis, bioinformatics tools and molecular dynamics simulations. The new findings aim to contribute to a better understanding of TRPC5 complex regulation during cell signaling processes in physiological and pathophysiological conditions. This understanding is crucial for exploring the TRPC5 channel as a potential target for novel strategies in pain management.

2 Literature review

2.1 TRPC subfamily

The TRPC channel subfamily has seven members: TRPC1, TRPC2, TRPC3, TRPC4, TRPC5, TRPC6, and TRPC7 divided into the two groups: Group 1 (TRPC1, TRPC4, TRPC5) and Group 2 (TRPC3, TRPC6, TRPC7) based on their structural homology, activation mechanisms and tissue distribution (Montell et al., 2002). TRPC1, TRPC4, and TRPC5 are widely expressed in various tissues and play important roles in processes such as smooth muscle contraction, cardiac function and kidney function. TRPC2 channel is not considered as a member of these groups as it is a pseudogene in humans. However, in rodents, it has an important function as the deletion of TRPC2 leads to a loss of sensitivity to pheromones, resulting in disrupted social and reproductive behaviors (Leypold et al., 2002).

In the central nervous system, TRPC1 channels are widely expressed and contribute to neuronal function. They play a role in synaptic plasticity and have been implicated in neurodegenerative disorders such as Alzheimer's disease (Lu et al., 2017). In sensory neurons, TRPC3 channels play a role in sensory transduction processes, including nociception. Increased expression and activity of TRPC3 were observed in animal models of epilepsy, suggesting its involvement in seizure generation in epileptic disorders (Kim et al., 2013). In the kidneys, TRPC6 channels are primarily located in podocytes, crucial cells for maintaining glomerular filtration barrier integrity. Mutations in TRPC6 have been associated with familial focal segmental glomerulosclerosis, a progressive kidney disorder characterized by renal disfunction (Winn et al., 2005).

TRPC3, TRPC6, and TRPC7, are primarily found in the central nervous system (CNS) and peripheral neurons. These channels are predominantly activated by diacylglycerol (DAG), thus this group is considered as DAG sensitive (Hofmann et al., 1999; Okada et al., 1999). Interestingly, subsequent studies have shown that TRPC4 and TRPC5 can also be activated by DAG, but their activation is tightly regulated by interaction with adapter proteins known as Na^+/H^+ exchanger regulatory factors (NHERF) (Storch et al., 2017). This suggests an overlap in the activation mechanisms between the two groups.

The most physiologically relevant mechanism of TRPC activation involves the stimulation of G protein-coupled receptors (GPCRs). The activation of phospholipase C (PLC) by GPCRs generates inositol trisphosphate (IP_3) and DAG. IP_3 triggers the release of calcium from intracellular stores, while DAG directly activates TRPC channels, resulting in

calcium influx into the cell (Clapham, 2003; Schaefer et al., 2000). Additionally, TRPC channels can respond to physical stimuli, including changes in temperature, mechanical stress, and osmotic pressure, further highlighting their diverse activation mechanisms (Bernal et al., 2021; Gomis et al., 2008).

2.2 Architecture of TRPC5 channel

TRPC5 exists in cell membrane in the form of symmetrically arranged tetramers, composed of four subunits that make up a central pore. Each subunit (Figure 2) is made of six transmembrane helices (S1-S6) and has intracellularly positioned C and N-terminal ends (Song et al., 2021). In addition to homomers, in native systems TRPC5 can also form heteromeric complexes with TRPC1 and TRPC4 (Goel et al., 2002). These distinct tetrameric forms of ion channels (TRPC5/C1, TRPC5/C4, TRPC5/C1/C4) exhibit differences in their sensitivity to activating stimuli, biophysical characteristics, functional roles, and distribution within cells or the entire organism (J. Kim et al., 2019; Strübing et al., 2001).

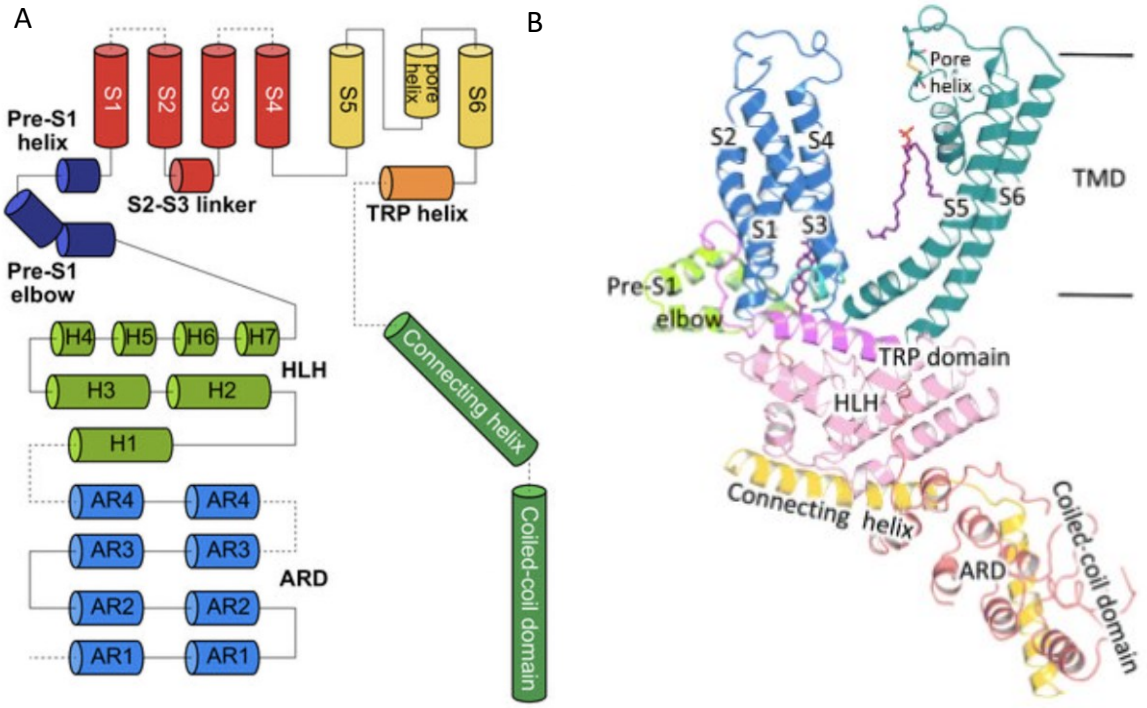

Figure 2: TRPC5 monomer structure. **(A)** *Linear representation highlighting the primary structural domains of the TRPC5 monomer, color-coded to correspond to the ribbon diagram (adapted from Duan et al., 2019).* ***(B)*** *Ribbon diagram portraying the detailed structural features of an individual subunit. S1-S6 represent transmembrane helices, while HLH denotes the helix-loop-helix structure linked to the N-terminal ankyrin repeats domain (ARD).*

Each TRPC5 monomer consists of a cytosolic domain and a transmembrane domain (TMD). The cytosolic N-terminal domain contains an ankyrin repeats domain (ARD) and a helix-loop-helix (HLH) region consisting of seven α helices. The C-terminus contains a coiled-coil domain with the rib helix (also known as connecting helix). TMD consists of six α helices, S1 to S6, along with the TRP domain, pore helix, pre-S1 elbow, pre-S1 helix, and an S2-S3 linker helix (Duan et al., 2019).

The central pore region of TRPC5 (Figure 3A) is composed of symmetrically arranged S5-S6 helices and pore helices from each of the four subunits. This pore region plays a critical role in determining the ion permeability of the channel. The permeability is governed by specific amino acid residues that form a selective filter and the lower gate of the pore. In the upper part of the pore, there are conserved residues G581 and N584, which together create the selective filter. These residues are responsible for allowing specific ions to pass through while excluding others. The lower gate of the pore is formed by residues I621, N625, and Q629, located in the narrowest region of the pore (Figure 3B). These residues act as a gate, controlling the opening and closing of the pore and regulating the flow of ions (Duan et al., 2019; Song et al., 2021).

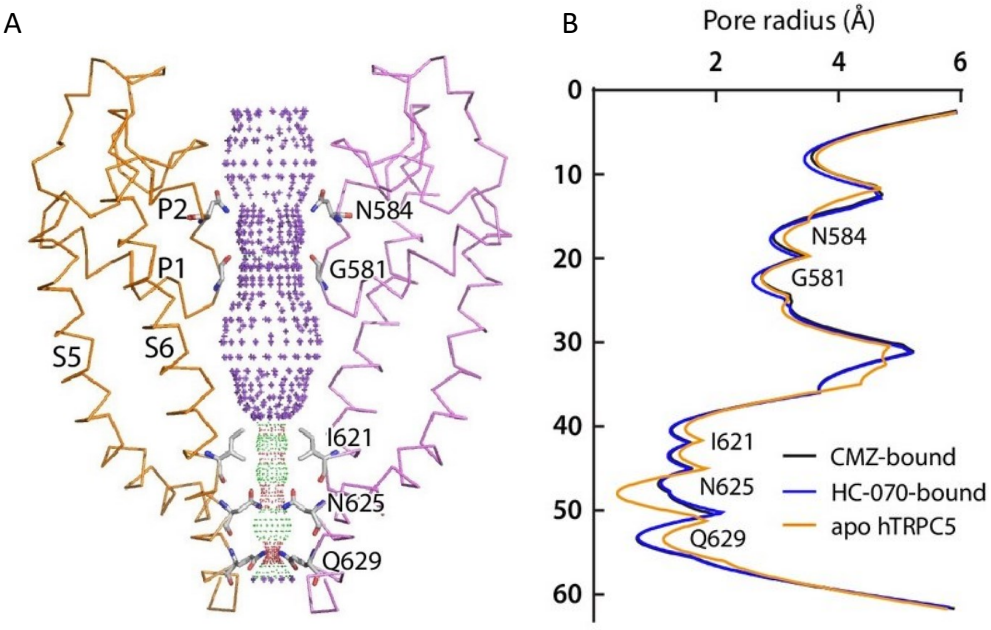

Figure 3: TRPC5 ion conduction pathway. (A) *Cross-sectional view of hTRPC5 pore, ribbons represents subunits A and C of the TRPC5 structure (PDB ID: 7D4P). The ion conduction pore within the pore is illustrated as dots, with key residues labelled. Dots correspond to pore radii of >2.8 Å (purple), 1.4–2.8 Å (green), and <1.4 Å (red).* ***(B)*** *Vertical presentation of calculated pore radii for CMZ-bound hTRPC5 (PDB ID: 7D4P), HC070-bound hTRPC5 (PDB ID: 7D4Q), and apo hTRPC5 (PDB ID: 7E4T). Y axis represents distance in Å along the pore (adapted from Song et al.,2021).*

2.2.1 Zn^{2+} binding site

In the N-terminal domain, situated between the ARD and the HLH region, there is a highly conserved region among the members of the TRPC family. Structural analysis of TRPC5 by cryoelectronic microscopy (cryoEM) identified a putative cation density in this specific region coordinated by amino acids H172, C176, C178 and C181 (Wright et al., 2020). The sequence motif formed by these residues resembles the zinc-binding site known from bacteria glucokinase, therefore identified density has been attributed to zinc (Miyazono et al., 2012; Wright et al., 2020). However, Song et al., prevented zinc binding by triple mutation of the involved residues (substitution to alanine) and observed that this did not affect TRPC5 activation by calcium or englerin A. Therefore, zinc binding at the N-terminal domain does not appear to have a significant effect on the gating of the channel (Song et al., 2021) and zinc's potential regulatory function on TRPC5 remain to be determined.

2.2.2 Ca^{2+} binding sites

TRPC5 undergoes tight regulation by both internal and external calcium ions. Activation of the TRPC5 channel and subsequent current generation require a minimum intracellular Ca^{2+} concentration of at least 10 nM (Okada et al., 1998). Elevating intracellular calcium levels to higher concentrations, such as 10 μM, leads to a significant increase in channel activation (Schaefer et al., 2000). In addition, even slightly elevated intracellular calcium levels, around 200 nM, can gradually induce TRPC5 activation independently of any other receptor stimulation (Shi et al., 2012; Zeng et al., 2004).

Moreover, when calcium is applied extracellularly, TRPC5 exhibits a substantial enhancement in ATP-induced current, showing the high dependence of TRPC5 activity on the presence of extracellular Ca^{2+} (Okada et al., 1998).

In a study by Duan et al. (2019), a cation-binding site within the voltage sensing-like domain (VSLD) on the S2, S3 was identified, with coordination through hydrogen bonding by several highly conserved residues E418, E421, N436, and D439. The authors did not specify the identity of this cation at the time, but assumed that it was Ca^{2+}. Identification of calcium ions within the VSLD cavity in ligand-bound and apo structures of the TRPC4 channel by Vinayagam et al., (2020) further supported this hypothesis and subsequent investigation confirmed it (Yang et al., 2022). This region also serves as a conserved Ca^{2+} binding site in various other TRP ion channels for example TRPM8 (Yin et al., 2019) and TRPA1 (Zhao et al., 2020; Zimova et al., 2018).

In a structural investigation by Guo et. al. (2022), researchers have revealed the existence of three distinct intracellular calcium-binding sites, CBS1–3 (Figure 4), within human TRPC3 and human TRPC6 channels. CBS1 and CBS2 are located within the C-terminal domain. CBS1 lies between the ARD and coiled-coil domain, while CBS2 is formed by residues on coiled-coil domain and the loop connecting rib helix with coiled-coil domain. CBS3 represents the site within VSLD mentioned earlier. Furthermore, CBS1 and CBS3 possess conserved calcium-binding residues across not only TRPC3 and 6 but also TRPC4, 5, and 7, implying that calcium possibly regulates TRPC5 channels at these sites. However, functional characterization of CBS1 in TRPC5 has not been documented so far (Guo et al., 2022).

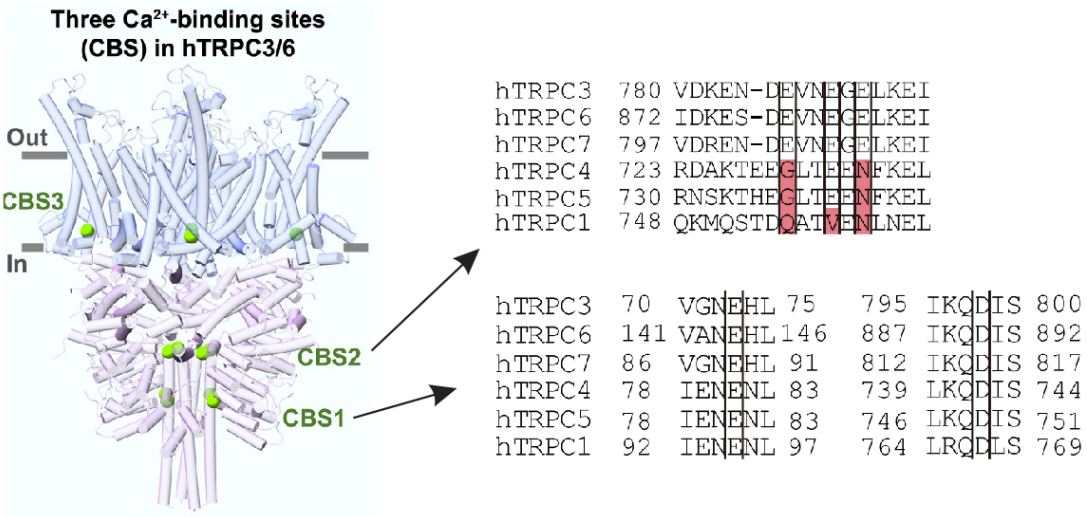

Figure 4: Conservation of Ca^{2+} binding in TRPC*: Overview of the three Ca^{2+} binding sites (CBS1/2/3) of human TRPC3 and human TRPC6. Note conservation of key amino acids among the members of the TRPC subfamily (adapted from Guo et al., 2022).*

2.2.3 NHERF association

The C termini of TRPC4 and TRPC5 channels contain a PDZ-binding motif, characterized by amino acid sequence VTTLR, which serves as the structural basis for their interaction with scaffolding proteins NHERF (Obukhov & Nowycky, 2004). This binding motif also houses a PKC (protein kinase C) phosphorylation site (T970, hTRPC5 numbering), known to play a crucial role in TRPC5 desensitization following receptor activation (M. H. Zhu et al., 2005). NHERF1 and NHERF2, adaptor proteins closely related in structure, have the capacity to form homo and heterodimers. They are characterized by two tandem PDZ domains and a C-terminal domain, facilitating their association with the actin cytoskeleton. Consequently, NHERF1 and NHERF2 proteins are believed to function as adaptors, linking integral membrane proteins (like TRPC5) to the cytoskeleton (Storch et al., 2017).

2.2.4 Calmodulin binding domain

TRPC5 is subject to a stringent regulation by calmodulin (CaM) through three distinct binding sites. One is situated in the N-terminal tail just prior to the transmembrane region, while the other two are located in the C-terminal tail.

The first, CIRB (Calmodulin and IP_3 Receptor Binding), is a common feature among all TRPC isoforms (Tang et al., 2001). The second calmodulin-binding site (CBII) in the C-terminus has been extensively studied, exhibiting a Ca^{2+} affinity over ten times greater than that of CIRB. CBII plays a crucial role in facilitating agonist-induced TRPC5 activation in a Ca^{2+}/CaM-dependent manner (Ordaz et al., 2005). Recent research on TRPC4 and CaM has shed light on how CaM binds to C-terminal rib helix of the channel (Figure 5), stabilizing it in a closed conformation, and suggesting a similar interaction potential with TRPC5 due to the high homology in the CIRB region (Vinayagam et al., 2020).

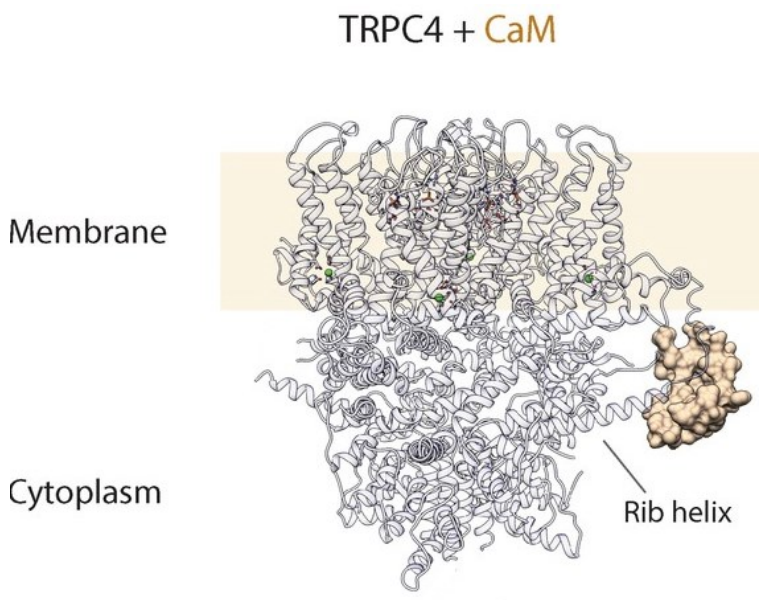

Figure 5: Cryo-EM structure of TRPC4 in complex with CaM (PDB ID:2LV6): *Interaction between calmodulin (CaM) and the rib helix of TRPC4 is depicted in a side view. The illustration features the CaM-bound TRPC4, with TRPC4 structure presented in a cartoon representation and CaM in a space-filling sphere representation. Although up to four binding sites are accessible for CaM, for clarity, only one binding event is shown in this representation (adapted from Vinayagam et al., 2020).*

2.2.5 Structural studies

In recent years, significant progress has been made in understanding the structural details of TRPC5. Up to this day, five structural research papers have been published with total of 10 molecular structures.

In the study by Wright et al., (2020), they uncovered that the LFW motif within the pore helix of TRPC5 plays a crucial role in binding the antagonist Pico145. They initially identified a density at the contact site between TRPC5 monomers, which resembled a phospholipid in structures without any ligands (apo structures). However, in the presence of Pico145, this density perfectly matched the shape and size of Pico145. This observation strongly suggested that the antagonist displaces previously bound phospholipids and exerts its influence on the pore helices of TRPC5 (Wright et al.,2020).

Building upon these findings, Song et al. (2021) demonstrated that the same lipid/Pico145 binding site can also accommodate HC-070, a potent TRPC5 inhibitor similar to Pico145. Furthermore, they detected a density at this binding site that resembled DAG in a cryo-electron microscopy map of human TRPC5 in complex with the inhibitor clemizole. High-performance liquid chromatography-mass spectrometry experiments revealed a significantly higher concentration of DAG in the purified protein sample compared to the purification control buffer. These discoveries led to the conclusion of a putative DAG binding site within the transmembrane region of TRPC5.

While it has long been known that ion channels can be directly regulated by the alpha subunit (G_{α}) of G-proteins (Jeon et al., 2012), conclusive structural evidence supporting this has been lacking. The most recent study solved the structure of TRPC5 in association with $G\alpha_{i3}$. The cryo-EM structure of the TRPC5-$G_{\alpha i3}$ complex revealed a 4:4 stoichiometry within lipid nanodiscs. $G_{\alpha i3}$ binds to an ankyrin repeat domain located approximately 50 Å away from the cell membrane. This finding contrasts with previous assumptions that Gα proteins directly interact with ion channels at the membrane interface. Electrophysiological experiments demonstrated that $G_{\alpha i3}$ has the ability to directly activate TRPC5 channels, with the crucial requirement of calcium and phosphatidylinositol-4,5-bisphosphate (PIP_2) as cofactors for $G_{\alpha i3}$ to achieve full channel activation. To gain structural insight into PIP_2 binding to TRPC5, attempts were made to incorporate PIP_2 into TRPC5 to resolve structure of TRPC5 in complex with PIP_2. However, these attempts were unsuccessful. To explore the potential binding conformation, the authors used molecular docking to predict the binding pose, followed by all-atom MD simulations of the PIP_2-bound TRPC5. To validate the interactions between PIP_2 and the surrounding residues within TRPC5, mutational electrophysiological assays were used. Remarkably, the electrophysiological measurements revealed that mutations in any of the five positively charged residues resulted in a significant reduction in PIP_2-induced currents in TRPC5. Based on these results, it has been proposed that the PIP_2 binding site on TRPC5 is positioned in proximity to the S2–S3 linker, S4–S5

linker, TRP helix, and the helix-loop-helix region. In conclusion, the study suggested that while $G_{\alpha i3}$ can bind to TRPC5 even in the absence of PIP_2, PIP_2 is essential for $G_{\alpha i3}$ to effectively gate the channel. This relationship between PIP_2 and $G_{\alpha i3}$ implies that the regulation of TRPC5 activity is dynamic and dependent on the local concentration of PIP_2 (Won et al., 2023). Recent studies by Duan et al., 2019 and Yang et al., 2022 are discussed in chapter 2.2.2.

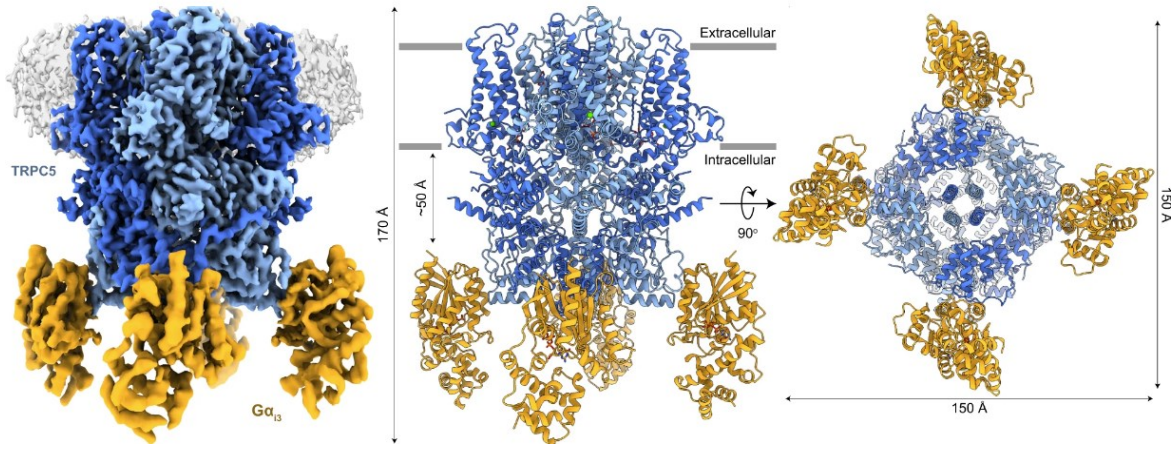

Figure 6: Cryo-EM structure of TRPC5 in complex with $G_{\alpha i3}$ (PDB ID: 2ODE): *Depiction of the TRPC5-$G_{\alpha i3}$ complex, featuring four bound $G_{\alpha i3}$ proteins. TRPC5 is presented in shades of blue, representing its two subunits within the opposing tetrameric assembly, while $G_{\alpha i3}$ is yellow. Grey shading indicates the nanodisc density. The image provides both side view (left, middle) and bottom view (right) (adapted from Won et. al. 2023).*

2.3 Modulation of TRPC5 channel

2.3.1 Voltage-dependent activation

TRPC5 channels are known to exhibit voltage-dependent behavior, meaning their activity can be influenced by changes in membrane potential. As other TRP channels, they are classified as voltage-gated ion channels according to Nomenclature and Standards Committee of the International Union of Basic and Clinical Pharmacology, although they do not possess the same structural characteristics and voltage-induced activation mechanisms as traditional voltage-gated channels (Obukhov & Nowycky, 2005). The current-voltage relationship (I-V) of TRPC5, as well as TRPC4, demonstrates a unique characteristic shape called double rectifying (Figure 7). This shape is distinct from the linear or outwardly/inwardly single-rectifying I-V relationships typically observed in many other ion channels (Zholos, 2014).

The double rectifying shape observed in TRPC5's current-voltage relationship is attributed to the presence of intracellular magnesium (Mg^{2+}). At depolarized potentials, Mg^{2+} blocks the channel by binding to the aspartate residue D633, which is located within the inner vestibule of the channel. This binding interaction slows down the outward flow of cations through the channel over the interval of 0–50 mV, contributing to the double rectification (Obukhov and Nowycky 2005).

Starting from negative membrane potentials, TRPC5 channel activity increases with membrane depolarization. This initial increase in channel activity is known as the activation phase. As the membrane potential becomes more positive, TRPC5 activity reaches a peak around -50 mV, exhibiting maximal conductance. This voltage range represents the voltage window where TRPC5 channels are most susceptible to opening. Subsequently, as the membrane potential increases, TRPC5 activity declines to a minimum around 20 mV, entering a state of reduced conductance also called as the inactivation phase. After reaching the minimum conductance, the activity of TRPC5 channel starts to increase linearly as the membrane potential becomes more positive. This subsequent increase in channel activity at very positive potentials is called a recovery phase and it is completing the voltage-dependent activation cycle of TRPC5 channels (Zholos, 2014).

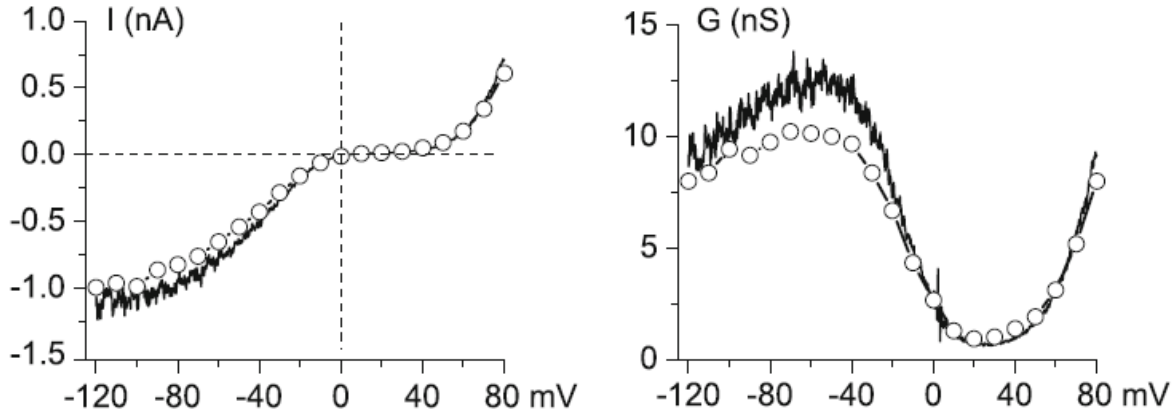

Figure 7: *The I-V (current-voltage) and G-V (conductance-voltage) curves of TRPC5 channels. The I-V curve (on the left) displays the typical doubly rectifying shape associated with TRPC5 channels. The G-V curve (on the right) illustrates an N-shaped pattern, which corresponds to the conductance of TRPC5 channels (adapted from Zholos 2014).*

2.3.2 Cold-induced activation of TRPC5

TRPC5 has been identified as an important molecular component for cold detection and adaptation to cold temperatures in the peripheral nervous system (Sadler et al., 2021; Zimmermann et al., 2011). It has also been implicated in mediating cold pain in odontoblasts

(Bernal et al., 2021). However, the thermal activation properties of TRPC5 remain relatively understudied compared to other thermosensitive TRP channels. While TRPC5 activation is known to be cold-sensitive, it remained unclear if this property is intrinsic to the channel itself or influenced by the cellular environment.

In the most recent study, decreasing the temperature resulted in prolonged mean open dwell times and a significant increase in the open probability (P_o) of the channel. In the absence of any agonists, the temperature dependence of P_o followed a sigmoidal pattern (Figure 8). Within the temperature range of 16–11 °C, the slope of the sigmoid curve was steep, indicating a pronounced increase in P_o. Below 8–5 °C, P_o reached saturation, suggesting that the channel reached its maximum open state under extremely cold temperatures. Thermodynamic analysis revealed significant changes in enthalpy and entropy, indicating substantial conformational changes associated with cold-induced gating of TRPC5 (Ptakova et al., 2022).

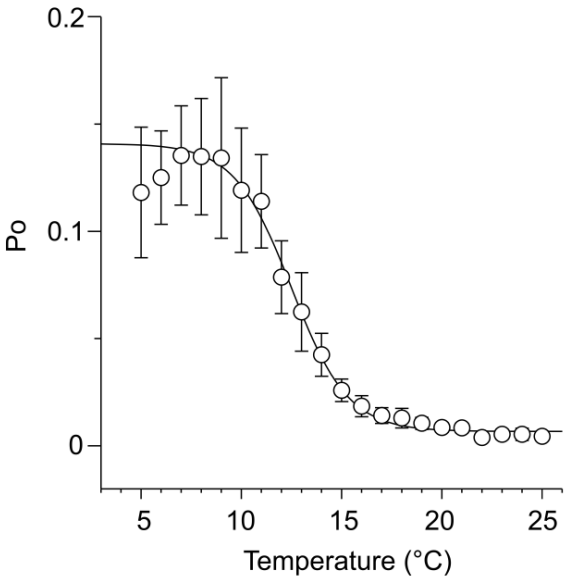

Figure 8: *Average open probability (P_o) of TRPC5 channel versus temperature characterizing cold sensitivity of TRPC5 channel, data points are means ± SEM (n = 18) (adapted from Ptakova et al., 2022).*

TRPC5 activity is regulated through phosphorylation at T970 via the PKC pathway. When T970A mutation was introduced, there was a notable reduction in the channel's cold sensitivity. Additionally, the mutant TRPC5 channel displayed significantly heightened activity at room temperature, and its response to temperature changes became less pronounced, with a threshold at 22 °C. Under colder conditions at 5°C, the mutant channel did not achieve the same level of activity as the wild-type (WT) channel. These findings

suggest that the PKC signalling pathway plays a direct and crucial role in the modulation of TRPC5 gating by temperature (Ptakova et al., 2022).

Overall, TRPC5 exhibits characteristics of an intrinsically cold-gated channel. The sensitivity of TRPC5 to cold temperatures is tightly dependent on the phosphorylation status of the protein and intracellular calcium homeostasis, further highlighting connections between various activation mechanisms.

2.3.3 Regulation by signalling pathways

Important and distinctive way of TRPC5 activation is not only by G-protein-coupled receptors described above but also by receptor tyrosine kinases (RTKs). The specificity and diversity of GPCR and RTK signalling allow for a precise modulation of TRPC5 activity in response to various extracellular signals. TRPC5 plays a role as a mediator between signalling molecules and downstream signalling pathways. GPCRs and RTKs initiate signalling cascades that not only affect TRPC5 but also interact with each other, resulting in a complex regulatory network (Kim et al., 2019).

A key player in this regulation is PLC, which is activated by GPCRs and RTKs. After activation, PLC breaks down PIP_2 into two signalling molecules: IP_3 and DAG. IP_3 binds to specific receptors in the endoplasmic reticulum (ER) membrane, leading to the release of calcium ions from ER stores, which modulate TRPC5 activity. This modulation is carried out by direct calcium binding to intracellular side of the transmembrane domain of TRPC5 and indirectly by calmodulin, which has predicted binding sites at C-terminal domain (Ordaz et al., 2005).

Furthermore, TRPC5 is also regulated by DAG (Figure 9). When TRPC5 is at its resting state, it associates with cytoskeletal structures via NHERF1/2 which makes the channel insensitive to DAG. However, when PIP_2 levels are depleted, it triggers a conformational change in the C-terminus of TRPC5 proteins. This change leads to the dissociation of NHERF1/2 proteins from the C-terminus of TRPC5. This allows TRPC5 to become sensitive directly to DAG (Storch et al., 2017). On the other hand, when PIP_2 levels are elevated PIP_2 binds to TRPC5 and it enhances the association between TRPC5 and NHERF1/2, maintaining the channel in an inactive state. DAG also activates PKC (protein kinase C) which phosphorylates and desensitizes the channel (M. H. Zhu et al., 2005). This dual role of DAG seems to be essential for the transient nature of TRPC5 activity which protects cells from calcium overload.

The mechanism of TRPC5 desensitisation has been elucidated just recently. PKC-mediated phosphorylation at T972 (*Mus musculus*, T970 in human TRPC5) and direct PIP_2 depletion both contribute to this process. PIP_2 has been shown to have a protective role in TRPC5 channel activity. The high affinity of TRPC5 channels for PIP_2 allows them to hold onto PIP_2 molecules, even when G protein-coupled receptors activate DAG production by triggering PLC-mediated PIP_2 hydrolysis. DAG molecules directly activate TRPC5 currents but also induce PKC-mediated phosphorylation of TRPC5 channels, particularly at the T972. The subsequent conformational change weakens the channel's interactions with PIP_2 and causes dissociation of PIP_2 from the channel. This phosphorylation-mediated inhibition opposes the activating effects of DAG, creating a balance between channel activation and inhibition (Ningoo et al., 2021).

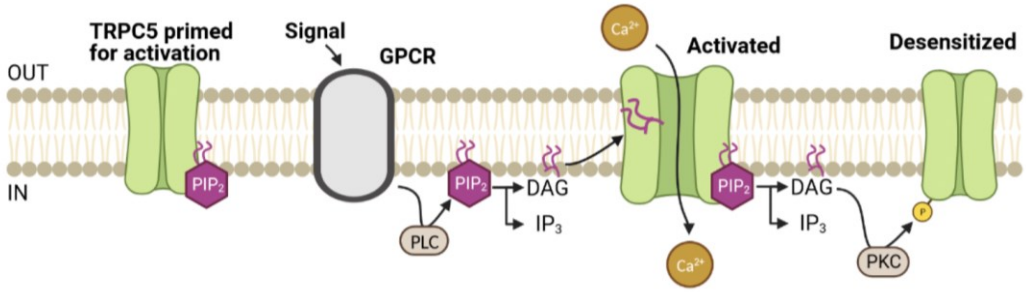

Figure 9: Schematic representation of TRPC5 modulation by G protein-coupled receptors. *After ligand binds to GPCR (depicted as signal) it in turn stimulates PLC to hydrolyse PIP_2 into IP_3 and DAG. IP_3 triggers Ca^{2+} release from ER. DAG activates PKC to phosphorylate TRPC5, causing desensitization. Non-hydrolyzed PIP_2 interacts with TRPC5, maintaining its activity (created in biorender.com).*

2.3.4 Agonists and inhibitors

The progress in TRPC5 research was held back for many years due to the absence of pharmacological tools that could specifically activate or inhibit this channel. As a result, TRPC5 activity was primarily stimulated indirectly through the activation of GPCRs. That changed after discovery of the specific agonist englerin A (EA) (Akbulut et al., 2015) and the specific inhibitor Pico145 (Rubaiy et al., 2017).

Englerin A (Figure 10 right), a natural product derived from bark of a tree *Phyllanthus engleri,* displayed an ability to specifically and potently inhibit the proliferation of renal cancer cells. This unique inhibition is achieved through an elevation in calcium ion influx, resulting in cellular Ca^{2+} overload. It has been proven that this was a result of

significant TRPC4/5 activation. Englerin A selectively activates TRPC5, TRPC4 and their heteromers (also heteromers with TRPC1) at low nanomolar concentrations and, so far, no other targets have been found to be modulated at these conditions (Akbulut et al., 2015). It is believed that EA binds to the transmembrane domain of TRPC5 causing a conformational change in the channels, facilitating calcium influx, but exact mechanism has not been discovered so far (Jeong et al., 2019).

Pico145 (Figure 10, left) has demonstrated potent inhibitory effects on TRPC1/4/5 mediated calcium influx without significantly affecting other TRPC family members or other ion channels. It is a small synthetic molecule that has been identified through a high-throughput screening approach aimed at finding compounds that can modulate TRPC channel activity (Rubaiy et al., 2017). Pico145 binds to a conserved lipid binding site between TRPC5 subunits, displacing phospholipids that in turn affect pore helices.

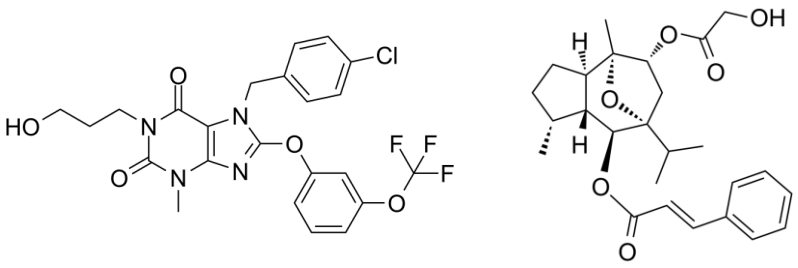

Figure 10: *Structures of Pico145 (left) and englerin A (right).*

2.4 Post-translational modifications of TRPC5 channel

Post-translational modification (PTM) represents a crucial aspect of molecular biology, encompassing a diverse set of chemical changes that proteins undergo after (or during) their synthesis within a cell. These modifications play fundamental role in the final structure and function of proteins including TRPC channels. It has been shown that various aspects of TRPC channel behaviour, such as gating, subcellular trafficking, protein-protein interactions, recycling, and protein architecture can be modulated by PTMs, including phosphorylation, N-glycosylation, disulphide bond formation, ubiquitination, S-nitrosylation, S-glutathionylation, and acetylation (Liu et al., 2020).

Among these PTMs, disulphide bond formations are notably significant. For instance, a pair of cysteines (C553 and C558) situated extracellularly in the pore loop between the S5 and S6 helices has been shown to be crucial for TRPC channel multimerization and plasma membrane trafficking (Jeong et al., 2019). Importantly, these cysteines also play a role in channel activation, facilitated by reducing agents that break the C553-C558 disulphide

bridge. This mechanism has implications in conditions like rheumatoid arthritis, where elevated levels of reduced thioredoxin in affected tissues activate TRPC5 channels, suppressing synovial fluid secretion. Blocking TRPC5 channels enhances secretory activity and counteracts thioredoxin-induced suppression (Xu et al., 2008).

Another pair of cysteines (C176 and C178), located within ankyrin repeat 4 at the intracellular N-terminus, serves as a probable site of S-glutathionylation, a modification that potently activates TRPC5 channels. This glutathionylation, occurring during oxidative stress, leads to sustained increases in cytosolic calcium concentration, resulting in cell toxicity and neurodegeneration, an important event in the pathogenesis of Huntington's disease (Hong et al., 2015).

2.4.1 Phosphorylation

Phosphorylation of proteins is a most common post-translational modification functioning as a molecular switch, enabling the activation or deactivation of proteins. It is a reversible process, orchestrated by protein kinases, which mediate the addition of a phosphate group (PO_4) to amino acid residues, mainly serine, threonine and tyrosine (Songyang et al., 1996). Although these residues are main target of protein phosphorylation, kinases can also phosphorylate other amino acids. Notably, serine residues account for 86.4% of phosphorylated sites, followed by threonine at 11.8%, while tyrosine phosphorylation, at 1.8%, is relatively rare (Nishi et al., 2014; Schwartz & Murray, 2011). Phosphorylation also less frequently extends to histidine and aspartate residues (N-phosphorylation), and these modifications tend to be less stable. Phosphate addition transforms the protein's characteristics mainly by altering its structure. As a result, phosphorylated amino acids gain the ability to interact with molecules that can engage with other proteins, enabling the assembly and disassembly of protein complexes, an appropriate example is already mentioned interaction between TRPC5 and NHERF where NHERF1/2 binds to the protein through threonine (970) phosphorylation (Albert et al., 2007; J. Zhu et al., 2005). This regulatory mechanism plays an important role in cellular processes of protein synthesis, development, signal transduction, cell growth, cell division, and aging (Ardito et al., 2017)

Protein kinases are a diverse family of enzymes responsible for catalysed transfer of γ-phosphate from ATP to amino acid residues (Cohen, 2003). Activation or deactivation of kinase occurs in different ways: among others, through the kinase itself with a cis-phosphorylation/autophosphorylation or by binding with activator or inhibitor proteins. The catalytic domain of a protein kinase comprises two subdomains, N-terminal and C-terminal,

connected by a peptidic linker forming an active site (Schwartz & Murray, 2011). Kinase activity can potentially modify up to 30% of human proteins, exerting regulatory control over numerous cellular pathways, particularly to a signal transduction. Kinases are known not only for their vital signalling roles but also for their capacity to modulate signal transduction amplitudes (Hornberg et al., 2005). Most kinases target both serine and threonine (serine/threonine kinases; STKs), while others focus on tyrosine (tyrosine kinases; TKs), and some can phosphorylate all three types (dual-specificity kinases; DSKs). Protein phosphatases serve as the counterparts to kinases, working in opposition to these enzymes by catalysing the removal of phosphate groups from phosphoproteins through hydrolysis of phosphoric acid monoesters (Zhang et al., 2002). This enzymatic action quickly reverts the protein to its non-phosphorylated state, a process that occurs more rapidly than kinase-mediated phosphorylation (Li & Stern, 2005).

Quantitative Post-translational Modification (qPTM) analysis, driven by the capabilities of mass spectrometry, represents an important step of modern proteomics research. One of the most advanced techniques within the mass spectrometry is tandem mass spectrometry (MS/MS), which allows researchers to not only identify the specific PTMs present on proteins but also quantify their abundance. In addition to experimental techniques, computational methods have been harnessed in qPTM analysis. Machine learning algorithms and bioinformatics tools are employed to predict potential phosphorylation sites on proteins, offering a more comprehensive understanding of the potential regulatory networks. These predictive models take into account various factors such as sequence motifs, structural information, and experimental data, enhancing our ability to decipher the intricate world of PTMs. As of right now qPTM database is home to 11,482,533 quantification events over 660,030 phosphorylation sites distributed across 40,728 proteins, all captured under 2,596 unique experimental conditions (Yu et al., 2023).

An example of the impact of phosphorylation on TRPC channels can be shown on the TRPC3 channel, precisely in the moonwalker mouse mutant. This mutation is characterized by cerebellar ataxia and abnormal Purkinje cell development accompanied by motor and coordination defects. This phenotype is attributed to a substitution point mutation at Thr635 for alanine (Thr646 in human TRPC3), resulting in reduced PKC-mediated phosphorylation of TRPC3 in moonwalker. The mutated TRPC3 channel exhibits abnormal gating, ultimately leading to the death of Purkinje cells (Becker et al., 2009).

2.4.2 TRPC5 phosphorylation

In the context of TRPC5 only three out of 164 potentially phosphorylatable serine, threonine, or tyrosine residues have been found to have an impact on TRPC5 function, so far. Zhu and colleagues studied desensitisation of TRPC5 after its indirect activation by carbachol, an agonist of muscarinic receptors (GPCRs). This desensitization in TRPC5 was found to be effectively prevented by the use of PKC inhibitors. Through point-mutation investigation of the possible PKC phosphorylation sites, one particular residue, Thr972 (Thr970 in human TRPC5), was identified. Substituting Thr972 with Ala led to a significant reduction in the extent of desensitization of TRPC5 (Zhu et al., 2005).

More recently, Sung et al. (2011) identified two more phosphorylation sites through similar approach. They investigated PKA (protein kinase A) and its role in TRPC5 modulation. They discovered serine residues (S794 and S796) at the distal C-terminus, which are phosphorylated by PKA, leading to the inhibition of TRPC5 currents with no apparent changes in TRPC5 surface expression levels (Sung et al., 2011).

By discovering additional phosphorylation sites on TRPC5, we can gain a more comprehensive understanding of the regulatory mechanisms that govern this channel's activity. These findings not only contribute to our knowledge of cellular signalling but also hold potential implications for therapeutic interventions, as targeting specific phosphorylation sites could be a viable strategy for modulating TRPC5 function in various pathological conditions, including neurodegenerative diseases and pain states.

3 Aims of the thesis

1) Based on available high-throughput bioinformatics and mass spectrometry data, select potential phosphorylation sites of the TRPC5 channel for functional characterization.

2) Prepare the *TRPC5* DNA mutants of selected sites via site-directed mutagenesis using appropriate PCR primers.

3) Characterize the parameters associated with voltage- and agonist-induced responses of heterologously expressed WT *TRPC5* in HEK293T cells using whole-cell electrophysiological techniques.

4) Functionally characterize the impact of the TRPC5 channel mutations using electrophysiological techniques.

5) Characterize cell surface expression of the residues identified in (4) as possible sites of TRPC5 phosphorylation and quantify membrane fraction using biotinylation assay.

6) Characterize structural role of the residues identified in (4) as possible sites of TRPC5 phosphorylation and use molecular dynamics simulations to determine how these residues may be involved in the regulation of ion channel activity.

4 Materials and methods

Solutions for Horizontal Electrophoresis

TAE Buffer (50x Concentrated)

- 2 M Tris base
- 1 M acetic acid
- 50 mM EDTA
- Diluted 50x before use

Solutions for Cell Cultivation

Phosphate Buffer (PBS)

- 137 mM NaCl
- 2.7 mM KCl
- 1.47 mM KH_2PO_4
- 4.3 mM Na_2HPO_4
- pH 7.3 (adjusted with NaOH)

LB Medium (Lysogeny Broth Medium)

- 0.5% (w/v) yeast extract
- 1% (w/v) peptone
- 0.26 M NaCl

Versene's Solution

- PBS
- 0.68 mM EDTA
- 87 µM trypsin
- pH 7.3

Solutions for Patch-Clamp Electrophysiology Technique

Extracellular Solution

- 160 mM NaCl
- 2.5 mM KCl
- 2 mM $MgCl_2$
- 1 mM $CaCl_2$
- 10 mM HEPES
- 10 mM glucose
- pH 7.4 (adjusted with NaOH)
- Osmolality 320 $mmol \cdot kg^{-1}$

Intracellular Solution

- 125 mM Cs-gluconate
- 15 mM CsCl
- 10 mM HEPES
- 0.5 mM $CaCl_2$
- 2 mM ATP
- 0.3 mM GTP
- pH 7.4 (adjusted with CsOH)
- Osmolality 286 $mmol \cdot kg^{-1}$

Solutions for surface biotinylation

PBS-CM

- PBS
- 1 mM $MgCl_2$
- 0.5 mM $CaCl_2$
- pH 8.0 (adjusted with NaOH)

Lysisbuffer

- 1% Triton-X100
- 150 mM NaCl
- 5 mM EDTA
- 50 mM Tris pH 7.5

SDS-PAGE and Western Blot Solutions

Running Buffer:

- 25 mM Tris
- 190 mM glycine
- 0.1% (w/v) SDS

Transfer Buffer

- 25 mM Tris
- 192mM glycine
- 20% (v/v) methanol

Tris Buffered Saline with Tween 20 (TBST)

- 150 mM NaCl
- 10 mM Tris HCl
- 0.01% (w/v) Tween 20
- pH adjusted to 7.4 with HCl

4x Sample Buffer

- 200 mM Tris HCl (pH adjusted to 6.8)
- 8% (w/v) SDS
- 40% (v/v) glycerol
- 50 mM EDTA
- 1.2 mM bromophenol blue
- 4% (v/v) β-mercaptoethanol (added before use)

Stripping buffer

- 1% SDS
- 62.5 mM Tris HCl, pH 6.8
- 0.8% beta-mercaptoethanol

4.1 Site of interest selection

To identify sites of interest, the online databases PhosphoNet (http://www.phosphonet.ca), EPSD (https://epsd.biocuckoo.cn), and qPTM (http://qptm.omicsbio.info) (all accessed in January 2022) were utilized. These databases provided a comprehensive array of mass spectrometry results and information on modified sites of the TRPC5 channel. Criteria for selecting specific residues for experimentation involved cross-referencing at least two databases, ensuring a high phosphorylation score, and verifying accessibility to kinases, while automatically excluding residues located in the transmembrane region. Subsequently, the Group-based Prediction System (GPS v5.0, https://gps.biocuckoo.cn) was employed specifically to predict potential phosphorylation sites influenced by extracellular signal-regulated protein kinases 1 (ERK1).

4.2 Direct mutagenesis

DNA constructs were prepared using the QuikChange II XL Site-Directed Mutagenesis Kit from Agilent Technologies. The plasmid pCMV6-AC which carries the gene encoding the wild-type hTRPC5 protein (OriGene Technologies), served as the template. Specific mutation primers (Table 1) were designed using the online tool QuikChange Primer (https://www.agilent.com/store/primerDesignProgram.jsp) and were synthesized by Merck. DNA amplification was carried out through polymerase chain reaction (PCR) in a Thermo-cycler (Eppendorf). The PCR reaction mixtures were prepared by combining components available in the kit, including 36.5 µl of distilled H_2O, 5 µl of 10× reaction buffer, 3 µl of Quick solution, 1 µl of dNTP mixture (10 µM), 1 µl of template DNA (100 ng), 1.25 µl of "forward" primer, 1.25 µl of "reverse" primer (both at 25 µM), and 1 µl of DNA polymerase (PfuUltra; 2.5 U/µl).

After completing the PCR (steps shown in the table 2), 1 µl of DpnI endonuclease was added, and the mixture was incubated at 37 °C for 1 hour. To verify the presence of the PCR product, horizontal electrophoresis was conducted. An agarose gel was prepared by mixing 30 ml of distilled water, 0.3 g of agarose, 600 µl of 50× concentrated TAE buffer, and 1.5 µl of peqGREEN (Peqlab). The prepared gel was placed in an electrophoresis chamber filled with 1× TAE buffer. A mixture of 5 µl of PCR product and 2 µl of loading buffer was applied to each well in the gel same as a 5 µl of a reference marker (1 Kb DNA Ladder, Geneaid).

The electrophoresis chamber was then connected to a power supply, applying a voltage of 80 V for 45 minutes. Following electrophoresis, the gel was examined under

a UV lamp in a darkroom, and if the presence of the plasmid of a specific size was confirmed, the PCR product was used to amplify plasmids in ultracompetent XL10-Gold E. coli cells (Agilent Technologies).

Table 1: *Direct mutagenesis primers used in experiments, the replacement of wild-type triplet for the desired mutation is highlighted in red*

Mutation	Primer (Forward+Reverse)
S193A	CAGCCTGCGCCACGCTCGCTCCCGACTG CAGTCGGGAGCGAGCGTGGCGCAGGCTG
S193D	CAGCCTGCGCCACGATCGCTCCCGACTG CAGTCGGGAGCGATCGTGGCGCAGGCTG
S195A	GCGCCACTCTCGCGCCCGACTGAACAT ATGTTCAGTCGGGCGCGAGAGTGGCGC
S195D	CCTGCGCCACTCTCGCGACCGACTGAACATCTAT ATAGATGTTCAGTCGGTCGCGAGAGTGGCGCAGG
S351A	ATAGCCTACCTGATCGCACCCAGGAGCAACC GGTTGCTCCTGGGTGCGATCAGGTAGGCTAT
S351D	GTCTATAGCCTACCTGATCGATCCCAGGAGCAACCTTGGGC GCCCAAGGTTGCTCCTGGGATCGATCAGGTAGGCTATAGAC
T755D	ACATCTCCAGCTTTCGGGATGAAGTGCTTGACCTC GAGGTCAAGCACTTCATCCCGAAAGCTGGAGATGT
Y144D	GAATTCACACCGGACATCGATCCCATCATGCTGGCTGC GCAGCCAGCATGATGGGATCGATGTCCGGTGTGAATTC

Table 2: *Table of individual PCR steps*

Step	Temperature (°C)	Duration	Number of repetitions
1	95	60 sec	1
2	95	50 sec	25
3	55	50 sec	25
4	68	16 min	25
5	68	10 min	1
6	4	∞	-

DNA was introduced into the cells using the heat shock method, following the protocol of the QuikChange II XL Site-Directed Mutagenesis Kit. Initially, agar plates were prepared by pouring a sterilized mixture (10 g Nutrient Agar No. 2, 250 ml of distilled water, and 500 µl of ampicillin) into culture dishes. The heat shock method was performed on ice, where 30 µl of E. coli cell suspension was combined with 2 µl of β-mercaptoethanol

and incubated for 10 minutes with occasional stirring. Then, 2 µl of the PCR product was added, and the cells were incubated on ice for 30 minutes. Microcentrifuge tubes containing the mixture were placed in a water bath at 42 °C for 45 seconds and immediately returned to the ice for 2 minutes. Subsequently, 200 µl of prewarmed (42 °C) LB medium was added to the tubes, and the entire mixture was placed in a shaking incubator (1 hour, 37 °C, 225–-250 RPM).

After incubation, the contents of the microcentrifuge tube were spread onto an agar plate, which was then placed in an incubator (16 hours, 37 °C, 5% CO_2) in a hanging position. Following incubation, several isolated colonies were aseptically collected from the plates and incubated in tubes containing 6 ml of LB medium with ampicillin (final concentration of 100 mg/l) in a rotating incubator (16 hours, 37 °C, 230 RPM).

The tubes were then centrifuged (7 minutes, 4 °C, 6000 × g, Centrifuge Rotanta 460R, Hettich Instruments), and DNA was isolated from the resulting pellet using the High Speed Plasmid Mini Kit (Geneaid, Biotech). The centrifugation steps were performed at room temperature with speeds of 13000 × g.

The DNA isolation was carried out according to the provided protocol. The isolated DNA was then tested using a spectrophotometer (NanoDrop One, Thermo Scientific) at a wavelength of 260 nm to determine the resulting DNA concentration. To confirm the introduction of the mutation, the isolation product was sent for sequencing to Eurofins Genomics. Sequencing primers (Table 3) were employed to assess the success and purity of DNA mutagenesis products, with a focus on specific target residues. Sequencing results were checked in the BioEdit program (Figure 11).

Table 3: *Sequencing primers for verification of hTRPC5 DNA mutagenesis products used in further experiments. Targeted amino acid region denotes the specific amino acid where the sequencing begins for each primer.*

Residue	**Sequencing primer (forward)**	**Targeted amino acid region**
S193	GAATTCACACCGGACATCAC	Y155 up
S195	GAATTCACACCGGACATCAC	Y155 up
S351	GAATTCACACCGGACATCAC	Y155 up
T755	ACTGGTTCAACAACACCTTC	R692 up
Y144	CGCAAATGGGCGGTAGGCGTG	M1 up

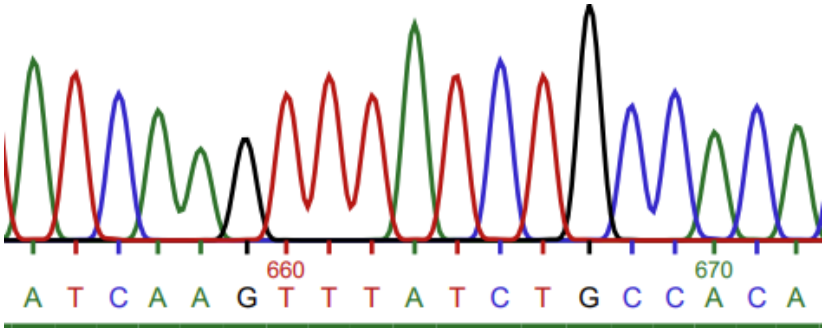

Figure 11: *An example of the sequencing result that displays sharp peaks and well-defined base sequences, ensuring the accuracy of the direct mutagenesis.*

4.3 HEK293T cells transfection

TRPC5 electrophysiology measurements were conducted on human embryonic kidney cells, HEK293T cell line (HEK293T, ATCC). The cells were transiently co-transfected with 300 ng of a plasmid encoding hTRPC5 wild type or its mutant constructs, along with 200 ng of a plasmid encoding green fluorescent protein GFP (pQBI 25 vector, TaKaRa), using magnet-assisted transfection (MATra). The cells were plated in 24-well culture dishes with 0.5 ml of 5% fetal bovine serum (FBS, PAN Biotech) in Opti-MEM (Thermo Fisher Scientific) to reach confluence of 60-80% on the day of transfection. The transfection mixture consisted of 50 µl of Opti-MEM, the appropriate amount of DNA, and MATra transfection reagent (0.1 µl of MATra per 100 ng of DNA). After adding the transfection mixture, the cells were placed on a magnetic plate in an incubator (40 minutes, 37 °C, 5% CO_2). Subsequently, the medium was removed, and the cells were passaged using phosphate-buffered saline (PBS) and Versene trypsin solution. Then, 1 ml of 5% FBS was added, adhered cells were resuspended using glass pipette and 1–-3 drops of this suspension was transferred to a glass-bottomed dish, coated with poly-L-lysine containing 2ml of 5% FBS in Opti-MEM. These prepared cells were placed in the incubator for 48–-72 hours before the start of the experiment. Individual GFP-labeled cells were selected for measurement.

For TRPC5 surface biotinylation, HEK293T cells were transfected with cDNA plasmid encoding wild-type or mutant C-terminally GFP-tagged human TRPC5 (pCMV6-AC-GFP vector, OriGene Technologies) using Lipofectamine LTX (Thermo Fisher Scientific). According to the manufacturer's protocol, two separate mixtures were prepared. The first mixture was a combination of 2 µl of Lipofectamine LTX and 150 ml of Opti-MEM. The second mixture comprised 1 µg of TRPC5-GFP-tagged DNA, 2 µl of Plus Reagent, and 150 µl of Opti-MEM. These volumes were adjusted for a single well

within a six-well plate. Just prior to transfection, the mixtures were merged, gently mixed by pipetting, and then transferred to a well within a six-well plate coated with poly-L-lysine. The transfection mixture was then allowed to incubate at room temperature for 15 minutes. HEK293T cells were cultivated in a six-well plate until they achieved an approximate 80% confluence. Subsequently, cells were harvested using standard procedure as described above (PBS wash, trypsin assisted dissociation, 5% FBS in opti-MEM resuspension). The prepared cells were then added into the transfection mixture with a dilution ratio of 1:10. The mixture was gently swirled, and the cells were incubated at 37°C in a 5% CO2 for 72 hours.

4.4 Electrophysiological measurements

Electrophysiological measurements were conducted using the patch-clamp method, enabling the recording of current responses in cells expressing specific ion channels at defined membrane potentials. The experimental setup included an Axopatch 200B amplifier (Axon Instruments, Inc; Molecular Devices) and an analog-to-digital converter, Axon Digidata 1550B (Axon Instruments, Inc; Molecular Devices), which digitized the acquired data for computer analysis. Current responses were recorded using pCLAMP 10 software, incorporating the Clampex 10 module, designed for both data acquisition and membrane potential control. Responses were recorded in whole-cell configuration.

Cells cultured on glass were placed in a dish containing ECS solution, and a reference electrode was immersed in the solution. Solutions, including control ECS and agonist mixtures, were applied to the cells using a gravity-based application system composed of seven solution containers connected to Teflon tubing, leading to a narrow bundle of capillaries ending in a single application capillary. The end of the capillary was positioned approximately 100 μm from the selected cell. A silver chloride measuring electrode was inserted into glass micropipettes made from borosilicate glass tubes (GB150F-8P, Science Products) using a Microforge MF-830 puller (Narishige) to achieve resistance ranging from 3 to 5 MΩ. During the experiment, the measuring electrode within the glass micropipette was positioned in close proximity to the cell using an MP-225 micromanipulator (Sutter Instrument). Application of negative pressure allowed membrane to adhere to the electrode and consequently rupture creating the whole-cell configuration.

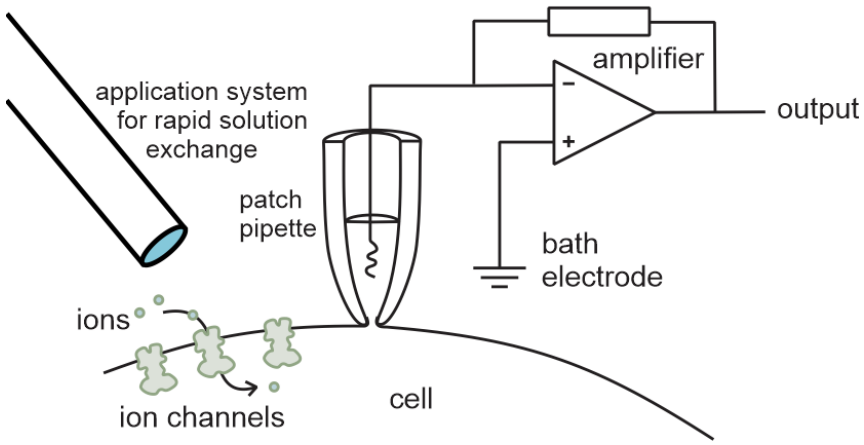

Figure 12: *Schematic representation of patch clamp setup in whole-cell configuration.*

4.5 I/V protocol and conductance analysis

The voltage activation of the TRPC5 receptor was investigated through 100 ms voltage steps ranging from -80 mV to +200 mV, with increasing amplitudes of +20 mV, applied in a control extracellular solution. Voltage-dependent activation parameters of the channel were estimated in the steady-state activation phase, always at the end (~90-–100 ms) of the voltage pulse. The relationship between the average amplitude of the membrane current (I) and the corresponding membrane potential (I/V) was depicted. After determining the reverse potential ($I(V_{rev}) = 0$), the conductance of the TRPC5 channel was calculated from the current responses using the (Formula 1):

$$G = I / (V - V_{rev})$$

where I is the current, V represents the membrane potential, and V_{rev} is the reverse potential. The obtained relationship was fitted in the tested cases with the Boltzmann function (Formula 2):

$$G = \frac{G_{max} - G_{min}}{1 + \exp\left(-\frac{zF}{RT}(V - V_{50})\right)} + G_{min}$$

where G_{max} is the theoretically maximum achievable conductance, G_{min} is the theoretically minimum achievable conductance, z is the gating charge, F is the Faraday constant ($F = 96{,}485$ C/mol*)* V is the voltage, V_{50} is the voltage at which the conductance reaches half of its maximum value, R is the universal gas constant ($R = 8.314$ J/(K·mol)), and T is the absolute temperature.

4.6 Surface biotinylation of eukaryotic cells with NHS-LC-LC-biotin

The whole process of Surface biotinylation of Eukaryotic cells with NHS-LC-LC-biotin was done in the cold room (4 °C). The cells were washed once with ice-cold PBS-CM, 2 ml for a well in a 6-well plate. Following the wash, the cells were incubated with 0.5 ml of biotin (Sulfo-NHS-LC-LC-biotin, Pierce) in a freshly prepared PBS-CM for 30 minutes, gently shaking. After biotin labelling, the cells were washed twice with PBS-CM containing 0.1% BSA to quench any unbound biotin. Subsequently, the cells were washed once with PBS at pH 7.4, and all PBS was carefully removed. After the washes, the cells were lysed with 0.5 ml of lysis buffer and incubated for 60 minutes, gentle shaking. While the cells were incubating, the neutravidin beads (Thermo Scientific) were prepared. 30 µl of neutravidin beads were washed twice in lysis buffer and then spun for 2 minutes at 2000 rpm. The cells were collected by using a cell scraper, and the cells were pipetted into test tubes. The test tubes were centrifuged for 10 minutes at 14000 g. After centrifugation, the supernatant was carefully pipetted into a new tube.

For further analysis, protein concentrations were measured using a BCA kit (Thermo-Scientific). Subsequently, equal amounts (1250 µg) of protein were added to the neutravidin beads, filling up to 1000 µl with lysis buffer. The samples were rotated overnight at 4 °C to ensure the effective binding of the proteins to the neutravidin beads. Following the overnight rotation, the beads were washed five times in lysis buffer to remove any non-specifically bound proteins. The proteins were then eluted in 60 µl of 2x Laemmli Sample Buffer (Bio-Rad, β-mercaptoethanol added) and the samples were incubated for 30 minutes at 37 °C to release the bound proteins.

4.7 SDS-PAGE

Mini-Protean TGX Stain-Free precast gels (10%) (Bio-Rad) were employed for the gel electrophoresis. The electrophoresis tank was filled with 1x running buffer. Protein samples were then denatured at 95 °C for 5 minutes and loaded into the wells. Electrophoresis was performed at 120 V until adequate separation of protein bands was achieved. Stain-Free technology allowed for direct visualization of protein bands under UV light, and results were documented.

4.8 Western blot

The PVDF membranes used in this Western blot were activated by immersion in methanol for 1 minute, followed by a brief wash with transfer buffer. The membranes were positioned on blotting papers that had been soaked with transfer buffer, with the gels placed on top. An additional blotter paper, soaked with transfer buffer, was placed atop the gel. These assembled "sandwiches" were then positioned within the blotting tank, ensuring that the membrane faced the positive pole. The tank was subsequently filled with transfer buffer and placed in a cold room at 4 °C. The blotting process was conducted at a constant voltage of 30V for a duration of 16 hours.

4.9 Immunolabeling

After the transfer, the membranes were briefly rinsed with distilled water, and then submerged in a 5% milk solution in TBST for 1 hour to block nonspecific binding sites. Following the blocking step the membranes were washed 3 times for 10-minute in TBST. The primary antibodies, mouse anti-GFP (diluted at 1:2000; OriGene, clone OTI2H8), in a solution of TBST for 1 hour at room temperature. Subsequently, immunoblots were treated with a horseradish peroxidase-conjugated goat anti-mouse IgG secondary antibody (diluted at 1:20000, Thermo Scientific) for 1 hour at room temperature. The membranes were then subjected to three additional 10-minute washes with TBST. The chemiluminescent substrate used for detection was SuperSignal West Femto Maximum Sensitivity (Thermo Scientific). The membranes were then visualized on ChemiDoc (Bio-Rad) using chemiluminescence automatic setting and analysed in ImageJ software.

4.10 PVDF membrane stripping

Membrane stripping was used to remove antibodies from PVDF membrane to subsequently visualize the cadherin as a control to TRPC5 biotynilation. The stripping buffer was warmed to 50 °C before being added to a small plastic container with a secure lid. The volume used was sufficient to completely cover the membrane. The entire setup was incubated at 50 °C for 30 minutes with periodic agitation. The membrane was then thoroughly rinsed under distilled water for 1 minute to eliminate any residual ß-mercaptoethanol, as its presence could potentially damage new antibodies. After rinsing, the membrane underwent 3x 5-minute wash in TBST, preparing it for the subsequent blocking step. Membrane was then checked

with chemiluminescent substrate if the antibodies were removed successfully. After this step membrane was probed again using already described immunolabeling method.

4.11 Molecular dynamics simulations

The apo structure of human TRPC5 (PDB ID: 7E4T) was retrieved from the RCSB protein database (https://www.rcsb.org/). In order to keep the channel compact during the simulation, we added the missing loops to the structure using Yasara software (ver. 18.12.7) built-in edit/build/loop function. A total of 5 missing loops on each of the 4 subunits were added between the residues (Tyr 118 - Gln 135, Asp 273 - Asp 286, Gln 386 - Asp 392, Asp 664 - Ser 706, Asn 731 - Thr 739). The build-in function of the UCSF Chimera software (ver. 1.14) Tools/Structure_editing/Build_structure/Modify_structure was used to create the structure with phosphorylated S193 (p-S193). Both the control structure and the p-S193 structure was than prepared for simulation by running the YASARA macro EM_runclean.mcr, that optimalize the hydrogen-bonding network and runs an energy minimization. Subsequent 30-ns-long molecular dynamics (MD) simulations were conducted using the Yasara "md_runmembranefast.mcr" macro, which initiates and runs the simulation under membrane conditions. Then, the "md_analyze.mcr" macro was applied to analyze and extract critical information from the simulated trajectories.

4.12 Statistical Analysis

The recordings from electrophysiological measurements were analyzed using Clampfit (version 10.7). Graphs were generated using SigmaPlot 10.0 software. Graphic adjustments and final figure preparation were performed using CorelDRAW X7 (version 17.6.0.1021). The average values presented in the graphs and text are expressed as mean ± standard error of the mean, where *n* represents the number of cells. The statistical significance of differences in data sets was determined using the t-test and ANOVA when it was appropriate ($P < 0.05$), unless otherwise stated.

5 Results

5.1 Selection of probable phosphorylation sites

In the investigation of TRPC5 regulation through phosphorylation, the initial focus was on the selection of phosphorylation sites identified using mass spectrometry. We screened modified sites of TRPC5 channel using online databases of protein post-translational modifications that include mass spectrometry results. We combined information from the PhosphoNet (http://www.phosphonet.ca), Eukaryotic Phosphorylation Site Database (EPSD, https://epsd.biocuckoo.cn) and quantification of Post-Translational Modifications (qPTM, http://qptm.omicsbio.info) databases and for further evaluation, only the sites listed in at least two of them were considered (Table 4). Of the eight such sites predicted, S794 and S796 were excluded because they had already been functionally characterized (Sung et al., 2011) and Y586 and Y628 because of their location in the transmembrane region, unreachable by kinases. Given that TRPC5 has recently been shown to play an important role in pain perception, it has been decided to include the possible target of phosphorylation by the extracellular signal-regulated protein kinases 1 (ERK1) to this study. ERK1 is an important kinase in pain processing (Ji et al., 1999) and its activity is clearly involved in pain perception and modulation via TRPA1 and TRPV1 (E. S. Schwartz et al., 2013). The possible sites of ERK1 phosphorylation were predicted utilizing Group-based Prediction System (GPS v5.0, http://gps.biocuckoo.cn). Of the three sites with the highest score, T144 was chosen because it is the only one resolved in the published structures of TRPC5 (Table 4). Thus, the full list of the sites for further functional characterization includes the following five residues: T144, S193, S195, S351 and Y755.

To examine the potential impact of phosphorylation on TRPC5, phospho-mimicking and phospho-null mutations were introduced into selected sites using site-directed mutagenesis, as described in detail in the Material and Methods section. The introduction of aspartic acid (D), in particular, served to mimic the negative charge of a phosphate group, simulating constitutive phosphorylation. On the other hand, the use of alanine (A) aimed to block phosphorylation at chosen sites by replacing the target amino acids with an unphosphorylatable alternative.

PTM databases			GPS 5.0 prediction	
PhosNET	EPSD	qPTM	ERK1	Score
			T144	11.4
S183				
S189				
S193	S193	S193		
S195	S195	S195		
	Y200			
	S205		S205	11.2
	S207			
	S231			
	T333			
	T336			
	Y348			
	S351	S351	S351	10.6
	S489			
	S490			
T498				
	Y524			
Y586	Y586			
Y628	Y628			
S666			S666	13.2
			S669	11.5
T680				
Y755	Y755			
	S769			
S794	S794			
S796	S796			
T816				
	S850			
T970				

Selected
Transmembrane
Not on structure
Characterized

Table 4: *Probable phosphorylation sites were selected by comparing query outputs to the three PTM databases PhosNET (PhosphoNet), EPSD and qPTM and the output of GPS prediction for hTRPC5 phosphorylation by ERK1. Selected sites are highlighted, as well as sites that met the selection criteria but were excluded because they are either in the transmembrane domain (marked as Transmembrane), are not resolved on published TRPC5 structures (marked as Not on structure), or their functional characterization has been published (marked as Characterized).*

5.2 Voltage dependent activation of WT TRPC5

To investigate voltage dependence, an I/V protocol (depicted in Figure 13A) was employed that involved a series of 100 ms voltage pulses applied to the cell in a control extracellular solution without the presence of chemical activators (Figure 13B). These experiments served as a control for measurements conducted on mutated TRPC5 channels. We measured average membrane current values at the end of the pulses, within the time interval of approximately 90–100 ms. These values were plotted against the applied voltage and the estimation of the reversal potential (V_{rev}) was performed from the current-voltage (I/V) characteristics. Conductance as a function of membrane voltage (G/V) was calculated (using the Formula 1, Chapter 4.5) for each recording. The individual I/V and G/V characteristics were averaged and graphically presented (Figure 13C,D).

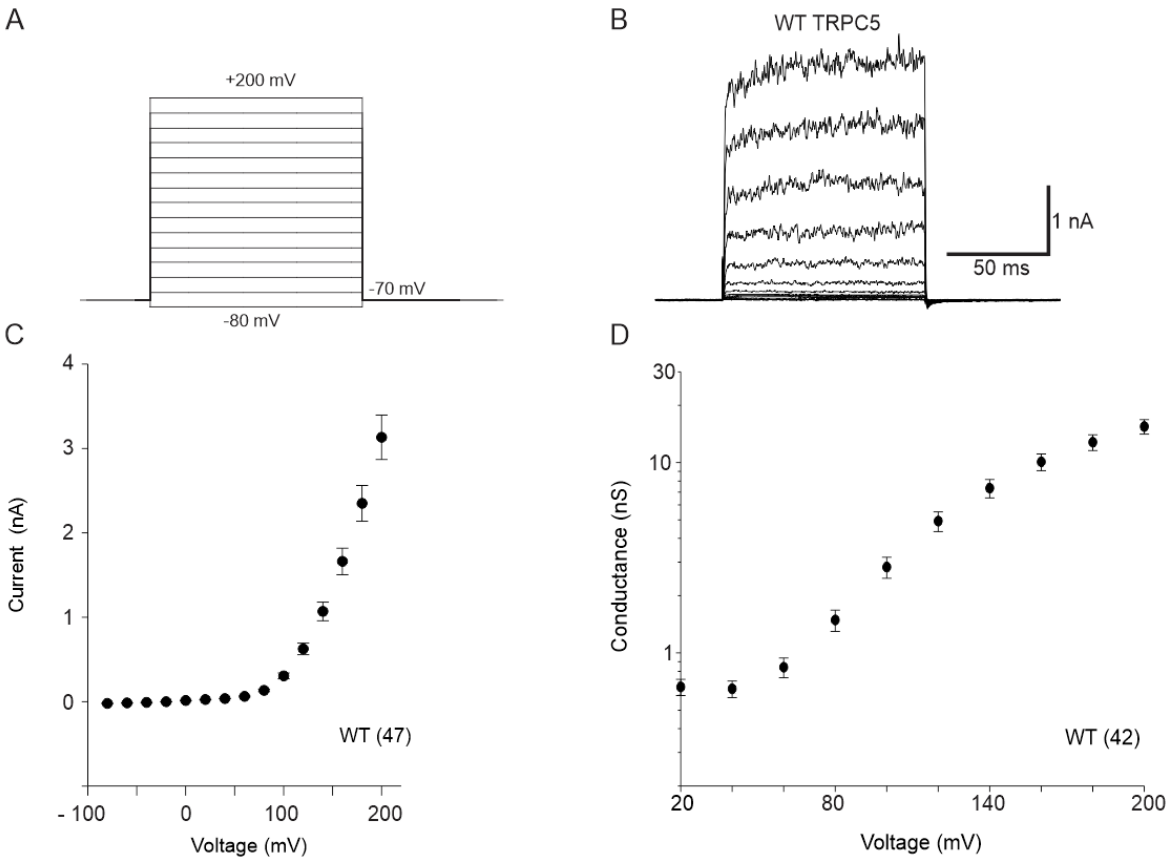

Figure 13: I/V protocol used on a wild-type hTRPC5 as control measurement.
(A) *Schematic illustration of the incrementally applied voltage pulses, starting from a minimum membrane potential of -80 mV and increasing in 20 mV steps up to a maximum of +200 mV, with the membrane potential maintained at -70 mV between pulses. A total of 15 pulses were delivered, each lasting 100 ms, with a 500 ms interval between them.* ***(B)*** *Representative current traces in response to I/V protocol (as in A) on WT TRPC5 channels.* ***(C)*** *The average current-voltage characteristics of WT TRPC5 channels (data points are means ± SEM, n indicated in brackets).* ***(D)*** *The mean conductance-voltage relationship averaged from individual recordings, as in B (data points are means ± SEM, n indicated in brackets).*

Control experiments demonstrated that the WT TRPC5 ion channels are inactive at negative potentials in the absence of agonists and the increase in activity occurs only upon depolarization above +60 mV (Figure 13C). Activation is characterized by a maximum current response of 3.3 ± 0.3 nA at +200 mV corresponding to the maximal conductance G_{max} = 15.5 ± 1.4 nS (n = 42), consistent with previous study from our laboratory (Zimova et. al 2022)

5.3 Voltage dependent activation of S193A/D and S195A/D

For characterization of voltage induced current from mutated TRPC5 ion channels, the same experimental I/V protocol as with the WT was utilized (Figure 14). At +200 mV, the average maximum voltage-induced current response for the phosho-mimicking mutation S195D did not differ from WT channels (1.8 ± 0.4 nA, n = 12). In contrast, the phospho-mimicking mutation S193D displayed a mean current of 0.5 ± 0.1 nA (n = 10), which is significantly lower than the currents obtained in control WT measurements. The phospho-null mutation S195A exhibited an average maximum current of 2.5 ± 0.6 nA (n = 9), which is not significantly different from WT channels. Interestingly, mutation S193A displayed an averaged maximum current of 8.2 ± 1.4 nA (n = 12), which is significantly higher than that of the WT channels (Figure 14C).

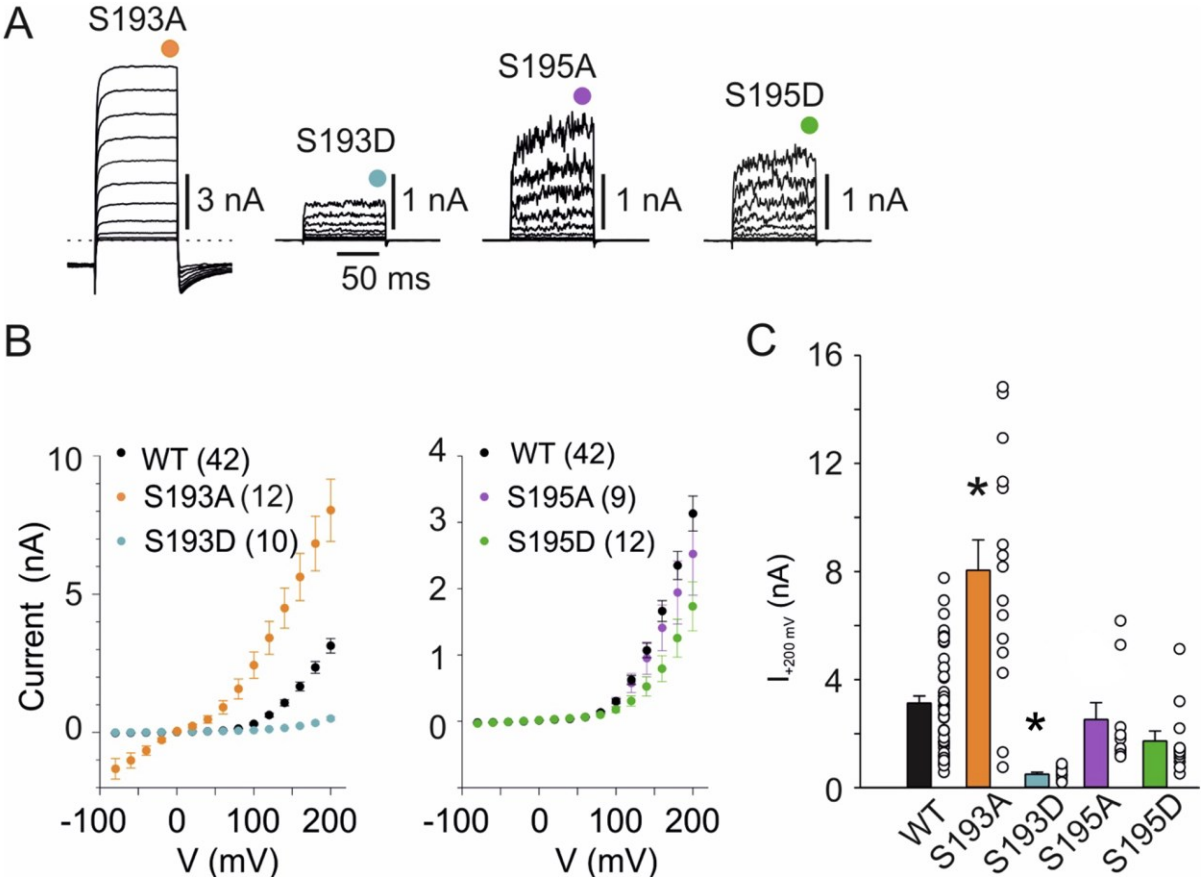

Figure 14: Phospho-mimicking and phospho-null mutations of S193 and S195 affect voltage-induced gating of TRPC5. *(A) Representative current traces of S193 and S195 mutants in response to I/V protocol (note the different scale for the mutation S193A).* ***(B)*** *Average current to voltage relationships of measurements as in A (data are means ± SEM, n indicated in brackets).* ***(C)*** *The average currents at +200 mV, bar graph represents means + SEM (*P<0.05).*

These findings reveal that both S195 mutations do not produce significant effects on the voltage-induced activation of TRPC5 channels. Conversely, mutations at S193 have a substantial impact on the channel's behavior. Phospho-mimicking mutation S193D leads to a reduction in voltage-induced responses activity, meaning the channels are less active at depolarizing voltages. In contrast, phospho-null mutation S193A causes a constitutively active phenotype, meaning that the channels are tonically active, even without voltage stimulation.

We further analysed mutations that differ from the wild type by determining their G-V relationship and estimated voltage-dependent parameters, where possible (Figure 15).

In the absence of an agonist, the activity of WT channels at negative potentials is minimal. Therefore, the analysis was focused primarily on positive potentials, where voltage-induced opening occurs. At +20 mV, WT channels exhibited a conductance of 0.64 ± 0.06 nS (n = 41), and the S193D mutation displayed a similar low value of 0.40 ± 0.08 nS (n = 10). Notably, the S193A mutation reached at +20 mV a significantly higher conductance of 10.3 ± 3.4 nS (n = 15). At +200 mV, WT displayed a conductance of 15.4 ± 1.4 nS (n = 41), a value significantly different from both S193 mutations. The S193A mutation reached 39.6 ± 5.6 nS (n = 15), and S193D had a conductance of 2.0 ± 0.3 nS (n = 10) (Figure 15A,B).

Next, the half-activation voltage (V_{50}) and the apparent number of gating charges (z) was determined for WT channels and the S193A mutant. Due to the low voltage activity of the S193D mutant, the data could not be reasonably fitted to a Boltzmann function (Formula 2, Chapter 4.5). There was no significant change in the apparent number of gating charges, with WT channels (z = 0.80 ± 0.05 *e,* n = 41) and S193A (z = 0.87 ± 0.04 *e*, n = 15). However, the S193A mutation caused a significant decrease in V_{50} to 117 ± 7 mV (n = 10) compared to WT V_{50} of 162 ± 3 mV (n = 41) (Figure 15C).

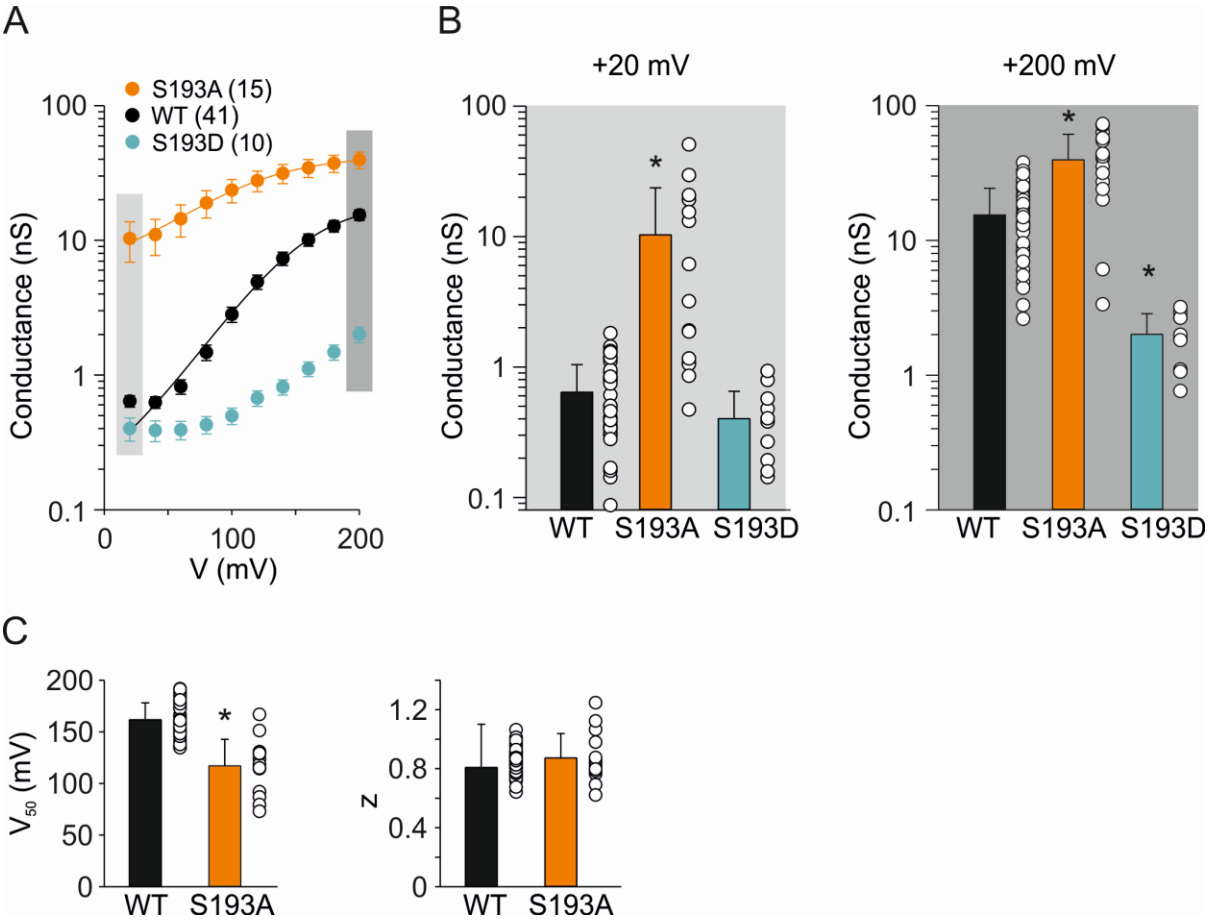

Figure 15: Phospho-mimicking and phospho-null mutations of S193 have opposite effects on the voltage-induced gating of TRPC5. (A) *Average conductances plotted against applied voltage obtained from recordings using an I/V protocol as in Figure 14A.* ***(B)*** *Vertical dot plots and bar graphs (means + SEM, n as in A, *P < 0.05) depicting the difference in conductance at +20 mV (light grey area) and +200 mV (dark grey area), corresponding to the data in (A) with matching color shading.* ***(C)*** *Vertical dot plots and bar graphs (means + SEM, n as in A, *P < 0.05) illustrating the half-activation voltage (V_{50}) and apparent number of gating charges (z) from experiments as in Figure 14.*

Taken together the S195 residue does not significantly contribute to voltage sensitivity of TRPC5 channel. Conversely, our data show that the S193 mutations severely affect the magnitude of voltage-induced current responses. While current responses are significantly increased in the phospho-null mutation S193A, the opposite is observed in the phospho-mimicking mutation S193D.

5.4 Voltage dependent activation of S351A/D, Y755D and T144D

In the next step S351A/D, Y755D and T144D were evaluated and compared to WT using I/V protocol (Figure 16). At +200 mV, S351A exhibited an average current of 3.5 ± 0.5 nA (n = 7), which is comparable to WT. S351D showed an average current of 2.5 ± 0.3 nA (n = 7), which is not significantly different from WT. Y755D displayed a response with an average current of 2.9 ± 0.4 nA (n = 7), which is comparable to WT. In contrast, the phospho-mimicking mutation T144D demonstrated a significantly lower average current of 1.3 ± 0.2 nA (n = 11) compared to the control WT. (Figure 16 B,C)

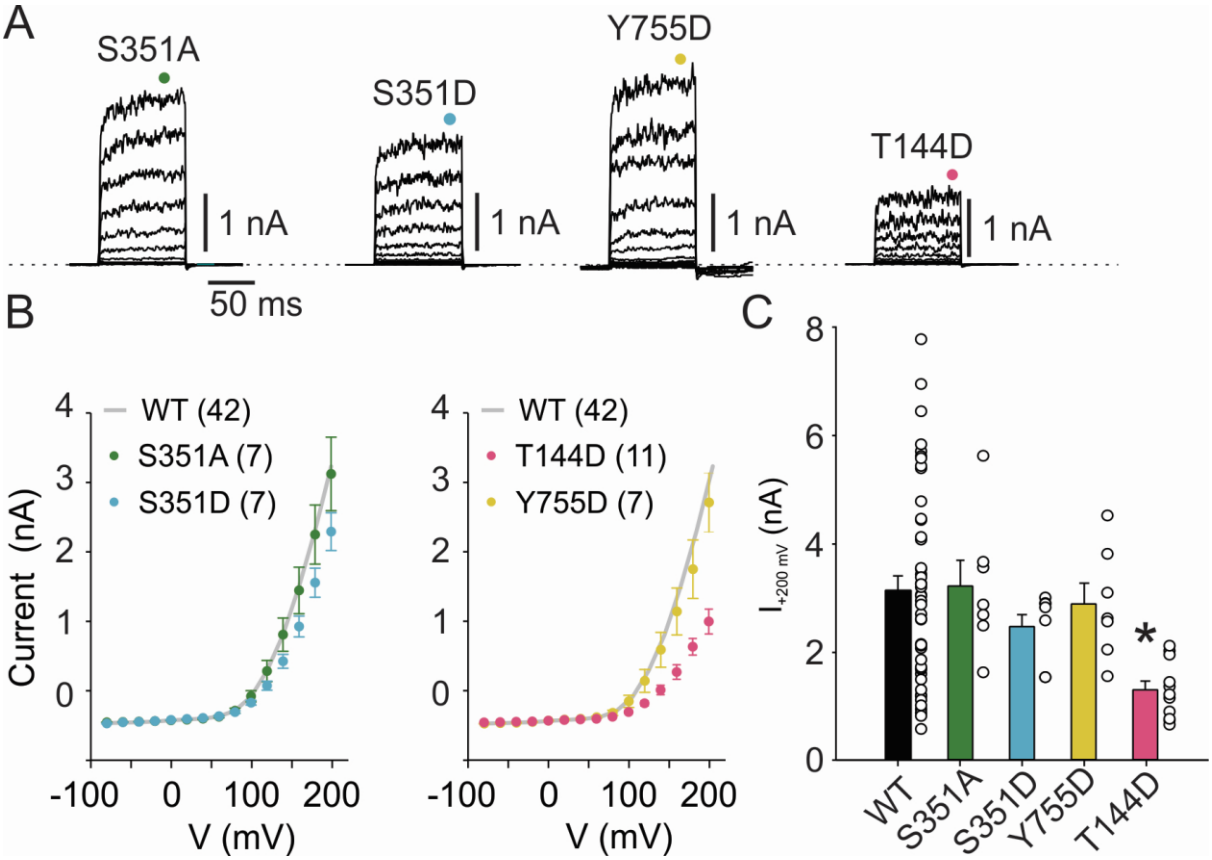

Figure 16: Current profiles of the S351, Y755, and T144 mutants of TRPC5 in response to I/V protocol. (A) *Representative current traces of S351, Y755, and T144 mutants in response to the I/V protocol.* ***(B)*** *Average current-to-voltage relationships of the measurements as shown in (A). Data are presented as means ± SEM, with the number of measurements indicated in brackets. WT is represented by grey solid line for comparison.* ***(C)*** *The point plot and bar graph of currents at +200 mV as means + SEM (n as in B, *P < 0.05).*

5.5 Agonist induced activation of WT TRPC5

In the next step agonist-induced gating was characterized, using potent selective agonist Englerin A (EA) which activates TRPC5 with an EC_{50} of 7.6 nM (Akbulut et al., 2015). Whole-cell currents were recorded using a linearly increasing voltage protocol (ramp protocol), where the voltage gradually increased from -100 mV to +100 mV at a rate of 1 V/s (Figure 17A). This protocol was repeated every 3 seconds while maintaining the membrane potential at 0 mV in between. Simultaneously with the ramp protocol, solutions were applied through the application system. Initially, there was a 30-second wash in extracellular control solution (ECS), followed by the application of 30 nM EA for 3 minutes. Subsequently, washout with ECS was applied for approximately 5 minutes or until the current stopped decreasing (Figure 17 B,C).

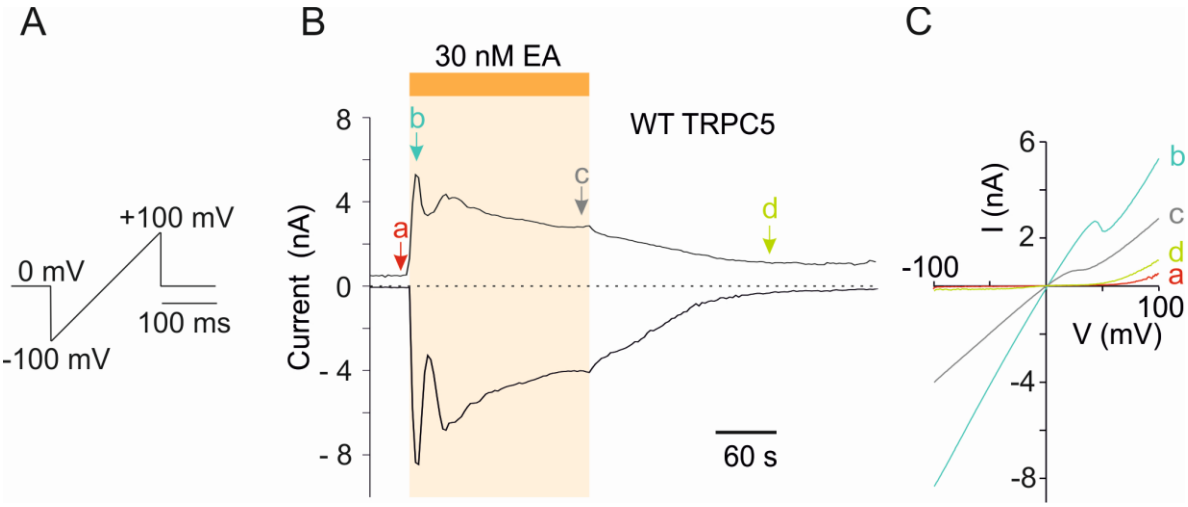

Figure 17: Control current responses of WT TRPC5 channels to Englerin A (EA) application (A) *Schematic representation of the applied ramp protocol.* ***(B)*** *Representative current traces of WT TRPC5 channels measured at +100 mV and -100 mV and plotted as a function of time. The horizontal bar above the record (orange) indicates the duration of EA application.* ***(C)*** *I/V relationship of a representative control measurement at time points denoted by letters a–d in B: (a) current before EA application, (b) peak current of EA application, (c) current after 3 minutes of EA application, and (d) current after 5 minutes of washout.*

The application of 30 nM EA in WT channels elicited a current response that reached its peak, averaging at 38 ± 6 s, with maximum amplitude of 3.5 ± 0.3 nA at +100 mV and -5.3 ± 0.4 nA at -100 mV (n = 16). In some cells, the current response exhibited slow oscillations during EA application after the first current peak was reached, likely due to the effect of calcium entry. Given that ECS contains 1 mM Ca^{2+}, the activity of TRPC5

can be substantially influenced by the Ca^{2+} ions passing through the opened channel pore (Schaefer et al. 2000). After reaching the maximum, the current response gradually declined, and at the end of the 3-minute application of EA, the average current reached 3.2 ± 0.3 nA at +100 mV and -4.3 ± 0.4 nA at -100 mV (n = 16). During the ECS washout, the current slowly returned to baseline values of 1.0 ± 0.2 nA at +100 mV and -0.4 ± 0.1 nA at -100 mV on average (n = 16) after 5 minutes.

5.6 Agonist induced activation of S193D and S195A/D

The ramp protocol was used to evaluate the responses of the S193 and S195 mutations to EA application (Figure 18). As cells expressing the S193A mutation could not endure a 3 minute-long exposure to EA, obtaining agonist-induced measurements of this construct was unattainable.

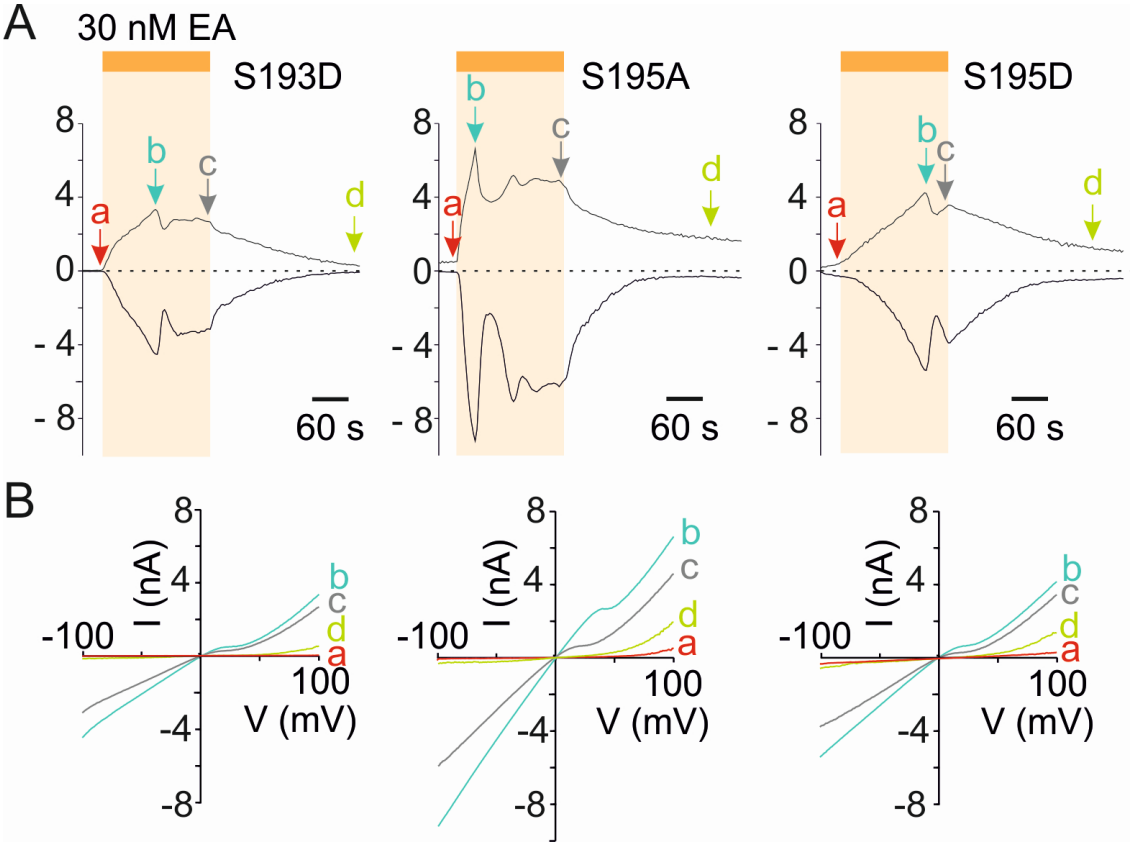

Figure 18: S193D and S195A/D responses to EA. ***(A)*** *Representative current traces of S193D, S195A, and S195D measured at +100 mV (top) and -100 mV (bottom) using the same protocol as in Figure 17A. The horizontal bar (orange) indicates the duration of EA application.* ***(B)*** *I/V relationship of representative measurements from time points denoted by letters a–d in A: (a) current before EA application, (b) peak current of EA application, (c) current after 3 minutes EA application, and (d) current after 5 minutes of washout.*

The evaluation of the TRPC5 mutants involved analyses of these parameters: Amplitude of the EA-induced peaks at +100 mV and -100 mV, magnitude of current responses after 3 minutes in EA, and the time of EA-induced peak. The EA-induced peak measured was the first peak after EA application, which, in the majority of cases, was also the largest. No statistically significant change in the amplitude of current responses compared to the WT was observed (Figure 19A), nor was there any notable difference in the current value after 3 minutes in EA (Figure 19B). However, the S193D and S195D mutations reached EA-induced peaks significantly later compared to WT (Figure 19C). Specifically, the average time of peak was 111 ± 15 s for S193D (n = 8), 99 ± 13 s for S195D (n = 6), in contrast to the WT's 28 ± 6 s (n = 16).

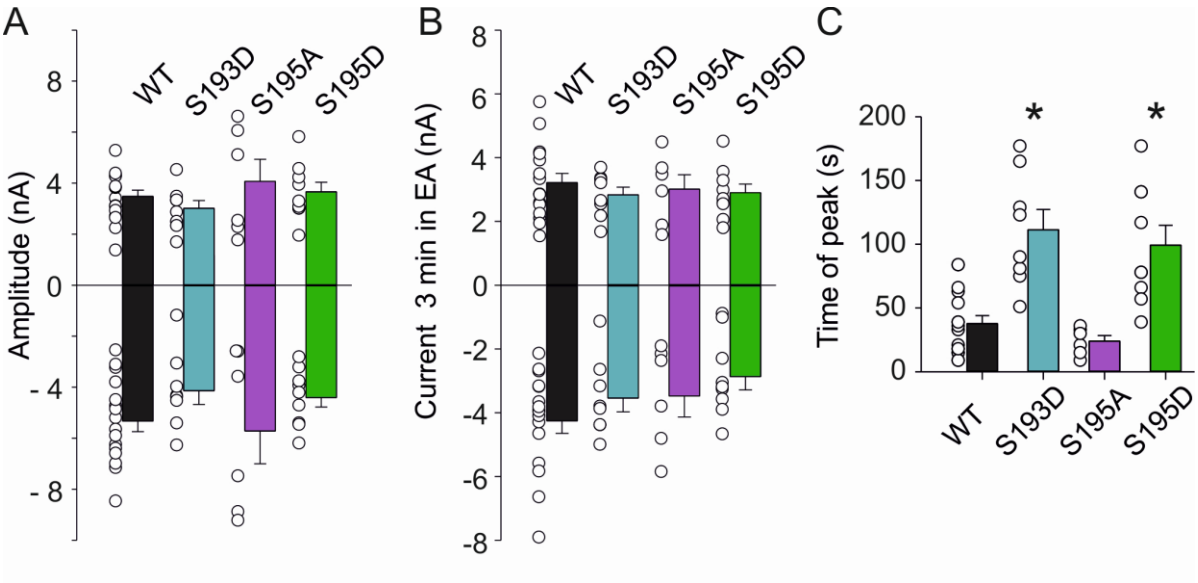

Figure 19: Analysis of EA-induced responses of S193D and S195A/D mutations: *The points represent the values of individual cells. Bar graphs represent means + SEM (WT n = 16, S193D n = 8, S195A n = 6, S195D n = 9)* ***(A)*** *Amplitudes of the first EA-induced peaks measured at +100 mV and -100 mV.* ***(B)*** *Magnitude of current responses at the end of EA application (after 3 minutes) from measurements as in Figure 18A, measured at +100 mV and -100 mV. Note that there is no statistically significant difference, suggesting that mutant channel functional expression is comparable to WT.* ***(C)*** *Time of the first EA-induced peak from measurements as in Figure 18. The times of peak of S193D and S195D are significantly delayed (*P<0.05).*

5.7 Agonist induced activation of S351A/D, Y755D and T144D

The voltage ramp protocol was next used to characterize S351A/D, Y755D, T144D mutations and their activation characteristics upon EA stimulation (Figure 20). The statistical analysis was used to evaluate the same parameters to characterize T144D, S351A/D, and Y755D mutations as were used for the S193 and S195 mutations.

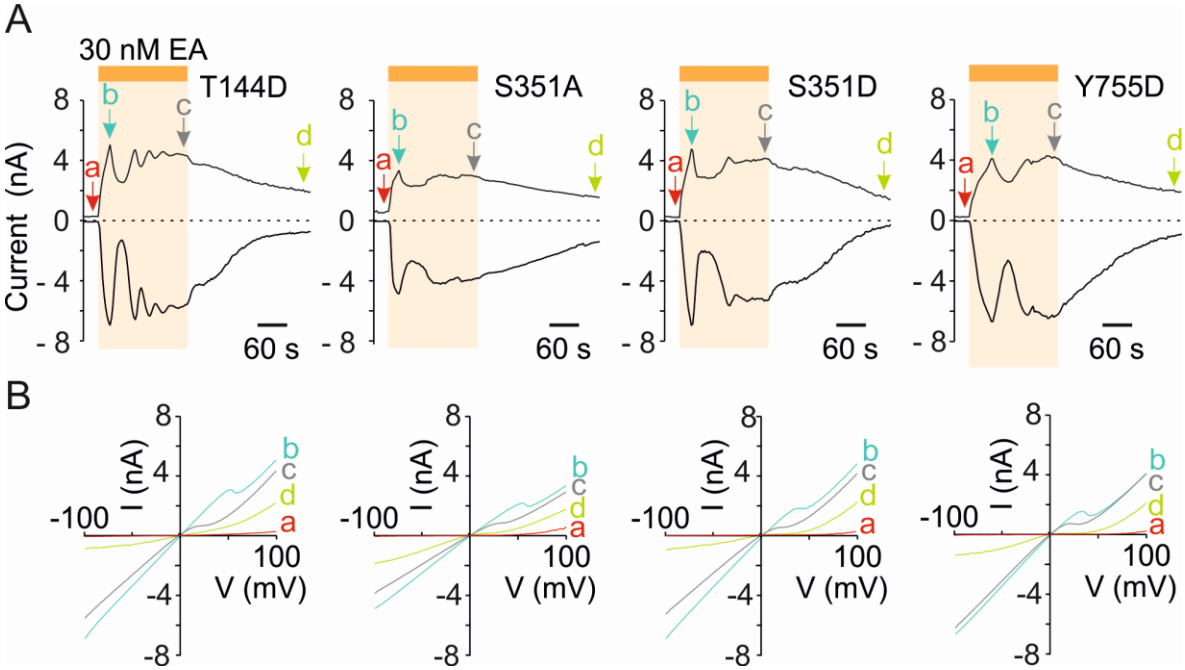

Figure 20: S351A/D, Y755D and T144D responses to EA. (A) *Representative current traces of T144D, S351A, S351D and Y755D channels measured at +100 mV (top) and -100 mV (bottom) using the same protocol as in Figure 17A. The horizontal bar (orange) indicates the duration of EA application.* ***(B)*** *I/V relationship of representative measurements from time points denoted by letters a–d in A: (a) current before EA application, (b) peak current of EA application, (c) current after 3 minutes EA application, and (d) current after 5 minutes of washout.*

The T144D, S351A/D and Y755D channels did not exhibit statistically significant differences in the investigated parameters of EA-induced responses compared to the WT (Figure 21). On the other hand, T144D exhibited significantly lower current levels in response to voltage during the I/V protocol (Figure 16C).

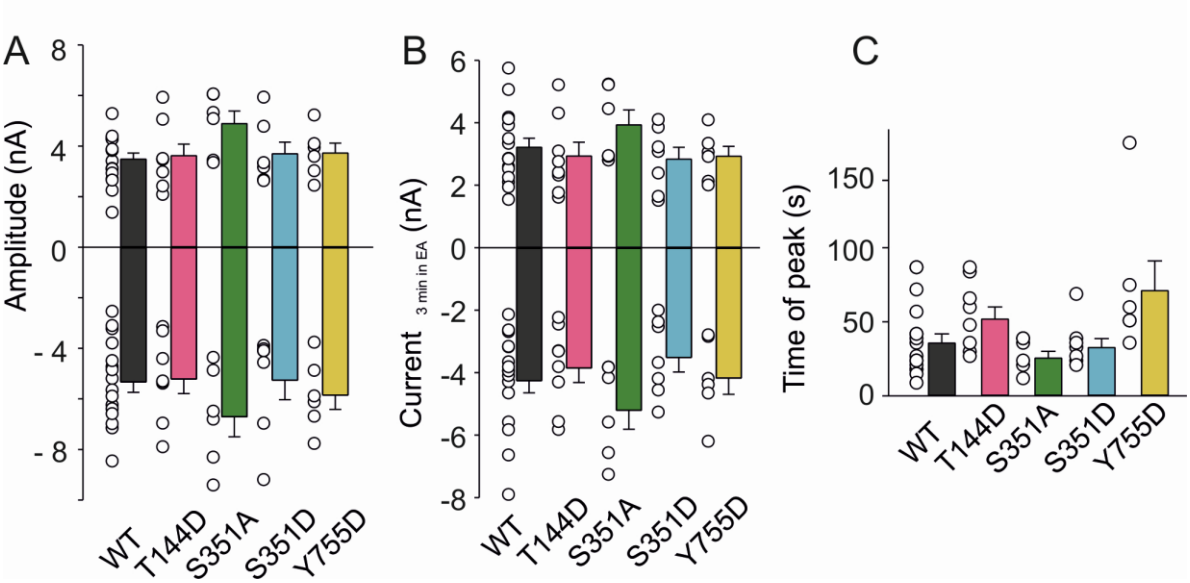

Figure 21: Analysis of EA induced responses of S351A/D, Y755D and T144D mutations. *The points represent the values of individual cells. Bar graphs represent means + SEM (WT n = 16 T144D n = 8, S351A n = 5, S351D n = 7 and Y755D n = 5), statistical analysis found no significant differences between tested groups* ***(A)*** *Amplitudes of the first EA-induced peaks measured at +100 mV and -100 mV.* ***(B)*** *Magnitude of current response at the end of agonist application (after 3 minutes) from measurements as in Figure 20A, measured at +100 mV and -100 mV. Note that there is no statistically significant difference, suggesting that mutant channels expression is comparable to WT.* ***(C)*** *Time of the first EA-induced peak from measurements as in Figure 20A.*

5.8 Characterization of S193A basal activity and impact of S193 mutations on cell surface expression

Basal current refers to the inherent tonic activity of an ion channel in its resting state, without any external stimuli. If a mutation induces constitutive activity, it becomes evident through an increase in basal current. After whole cell configuration formation, the basal current at -80 mV of WT channels was minimal unlike the basal current of S193A which was significantly different and showed large scatter with about half of the cells having values greater than -0.5 nA (Figure 22A).

A separate experiment with cells expressing the S193A mutation was performed to validate if this basal current is caused by the activity of the TRPC5 channels. After the whole-cell configuration formation, the membrane voltage was held at -70 mV and current was recorded continuously. The selective TRPC5 inhibitor Pico145 (IC_{50} = 1.3 nM) was applied at a concentration of 100 nM (Figure 22B). Notably, the consistent inhibition of the basal current was observed, confirming that high basal current in the S193A measurements is

caused by TRPC5 channel activity. The average current measured before the application of Pico145 in control ECS was -2.1 ± 0.5 nA (n = 5). Following the application of the inhibitor, there was a significant and consistent decrease, with the average current dropping to - 0.3 ± 0.1 nA (n = 5) (Figure 22C).

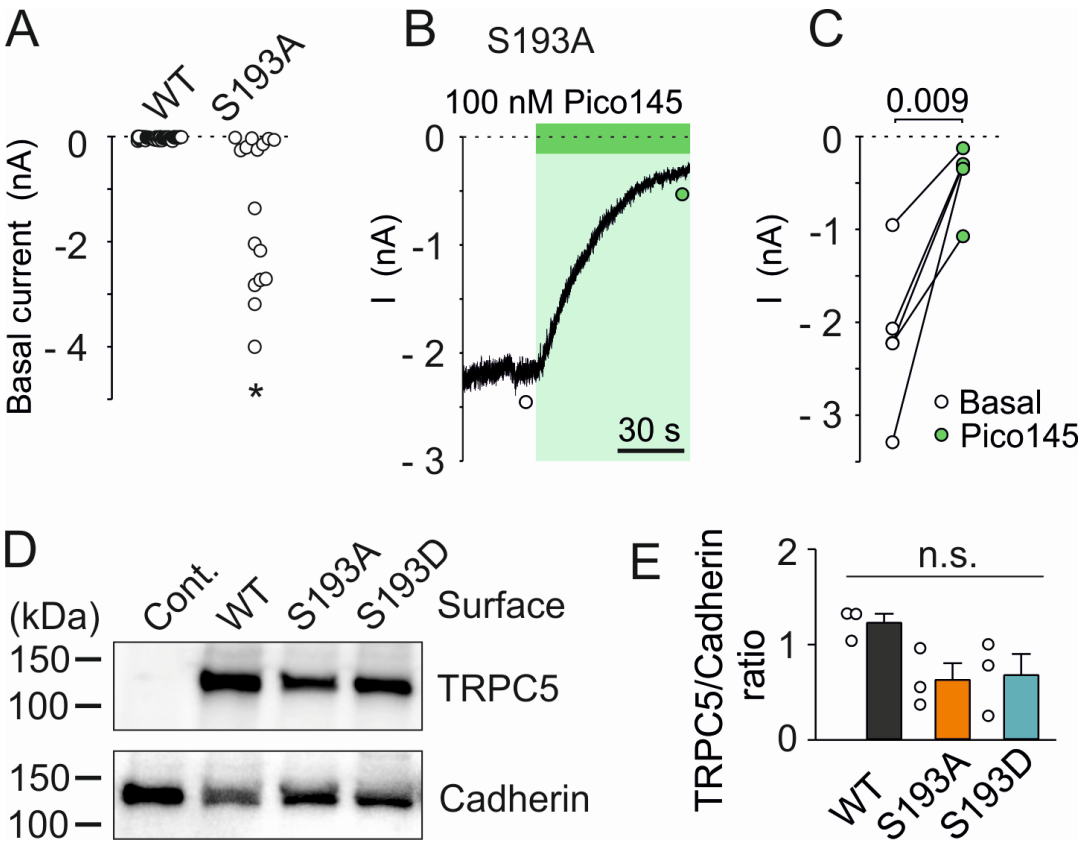

Figure 22: The increased activity of S193A can be inhibited by Pico145 and is not caused by increased translocation to the membrane. ***(A)*** *Points of data present the value of basal current measured at -80 mV in the control extracellular solution approximately one minute after establishing the whole-cell configuration (WT n = 43, S193A n = 16, *P<0.05).* ***(B)*** *Representative S193A current measurement at continuous voltage of -70 mV. Green bar represents application of the inhibitor Pico145. Green and white circles correspond to data collection time points in C.* ***(C)*** *Vertical point plot depicting the change in currents before and after Pico145 application on S193A measured as in B.* ***(D)*** *Representative Western blot, analysis was done using GFP antibodies illustrating cell surface and total TRPC5-GFP proteins in WT, S193A, and S193D mutant constructs expressed in HEK293T cells. Cell surface proteins were labeled by a biotinylation method and captured with NeutrAvidin agarose beads.* ***(E)*** *Point plot of individual analysis and bar graphs of TRPC5/cadherin ratios + SEM (n = 3, n.s.: non-significant)*

The increased basal activity in S193A may indicate a higher tendency for this mutant to translocate on to the plasma membrane. On the other hand, the results of the S193D mutation show lower (I/V protocol) or the same (EA measurements) membrane targeting as WT. To address this issue, biotinylation experiments were conducted. These experiments aimed to directly assess and quantify the surface expression differences among the WT, S193A, and S193D (Figure 22D,E). An anti-pan-cadherin polyclonal antibody served as a control in addition to the non-GFP-tagged TRPC5 control (anti-GFP primary antibodies were used). The results of 3 independent biotinylation experiments have shown that the quantity of channels present on the plasma membrane is roughly similar for WT, S193A, and S193D. This suggests that the observed functional changes in the S193 mutants, particularly the increase in basal current in S193A are likely attributed to the modified gating characteristics of the channels themselves, rather than a significant alteration in their translocation to the plasma membrane.

5.9 Molecular dynamics simulations of putative S193 phosphorylation

To comprehend the impact of the S193 phosphorylation on the channel's molecular structure, two 30ns-long molecular dynamics (MD) simulations were conducted based on the 7E4T structure of hTRPC5 published by Song et. al 2021. One with unmodified WT TRPC5 channel as a control, the second with the same TRPC5 channel structure but phosphorylated at S193 (p-S193) (Figure 23). Positioned in the helix-loop-helix region near the zinc binding site, S193 resides between the TRP helix and the rib helix. Moreover, it participates in the interaction between an adjacent subunit, contributing to inter-subunit interactions through H-bonds. We analysed snapshots from MD simulations and calculated the number of H-bonds between S193 or p-S193 and Q309 from the adjacent subunit. Notably, upon S193 phosphorylation a 3.6-fold increase in the probability of H-bond formation was observed (Figure 23D).

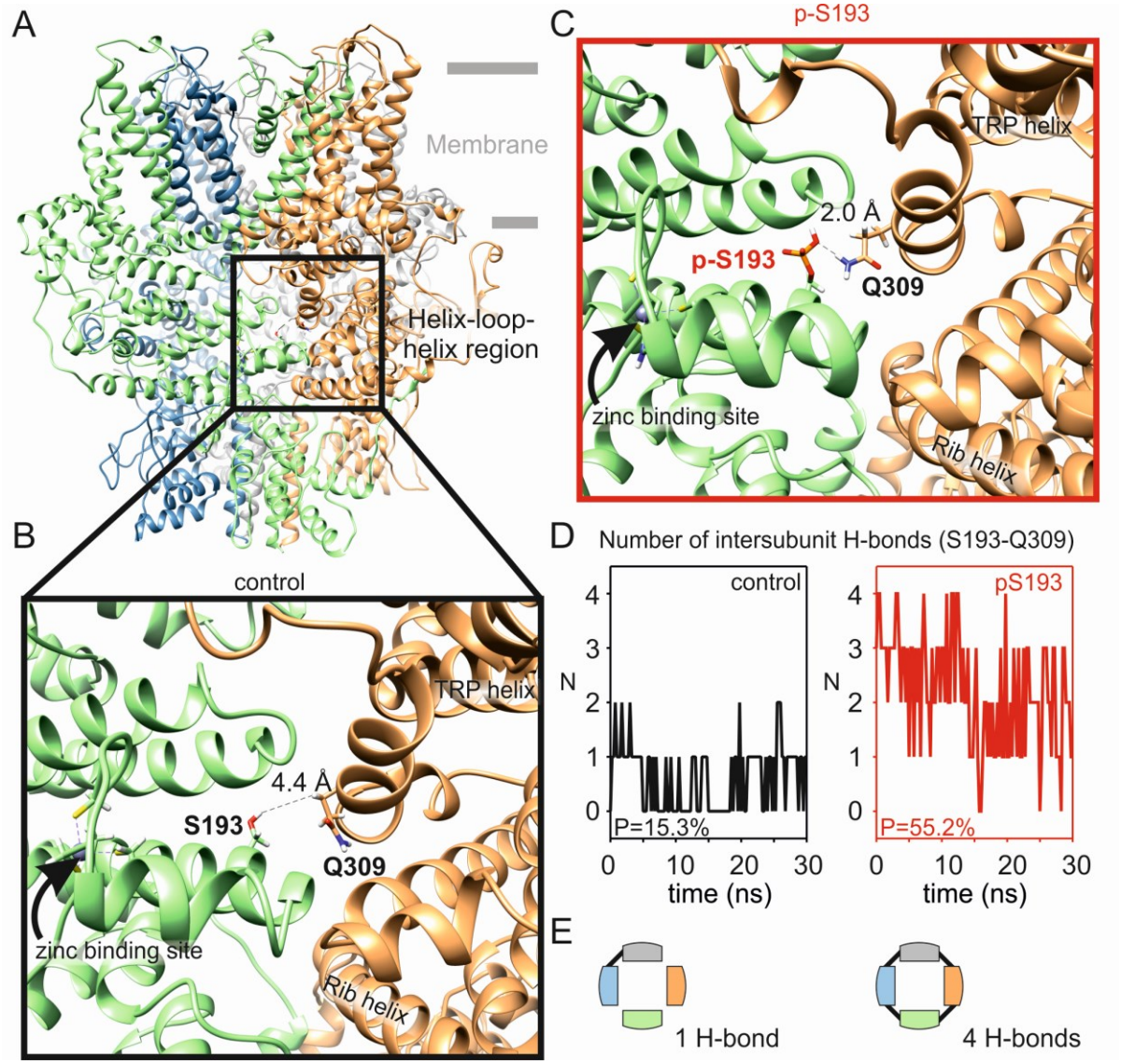

Figure 23: Phosphorylated serine 193 is more likely to form a hydrogen bond with glutamine 309 in the adjacent subunit. ***(A)*** *Molecular model of hTRPC5 based on the 7E4T structure at the end of a 30-ns-long MD simulation. Individual subunits are color coded.* ***(B)*** *Zoomed-in region of interest with the S193, Q309 residues and atomic distance indicated.* ***(C)*** *Phosphorylated S193 at the end of a parallel 30-ns-long MD simulation. H-bond indicated by atomic distance.* ***(D)*** *Number of intersubunit H-bonds between S193 (control) or phosphorylated S193 (pS193) and Q309 over the course of the MD simulations.* ***(E)*** *Schematic illustration of H-bonds between subunits of the ion channel tetramer.*

6 Discussion

The TRP channel family holds crucial relevance in the mechanisms of pain signalling. Unlike TRPV1 or TRPA1, which are directly activated by pungent compounds and have been studied in the context of pain for decades, the role of TRPC5 in pain pathways has only recently been confirmed (Sadler et al. 2021 and Bernal et al. 2021). As TRPC5 became promising target for pain management, there is an increasing need for research focused towards uncovering its activation mechanisms. This is particularly important because clinical research tends to be ahead of basic research. For example there is a TRPC5 inhibitor that is already being administered to humans in clinical trials against glomerular kidney diseases (https://clinicaltrials.gov accessed October 2023) while the underlying molecular mechanism is poorly described. A better understanding of TRPC5 modulation would definitely help in designing new TRPC5 modulatory molecules that lack the disadvantages of the current ones, such as low solubility, low selectivity for TRPC5, or high protein binding (Shen et al., 2023).

There is accumulating evidence that various pathophysiological conditions are accompanied by changes in TRPC5 expression (Alawi et al., 2017; Kuburas et al., 2021). A recent study (Adhya et al., 2023) shows increased TRPC5 expression in the dorsal horn of the spinal cord in rats experiencing mechanical allodynia due to diabetes. Notably, the study reveals that for diabetic neuropathy, a TRPC5 activator rather than an inhibitor yielded analgesic effects. This observation aligns with reports indicating that TRP channel agonists often induce ion channel downregulation mediated by various PKC isoforms (Bishnoi & Premkumar, 2013; Gada & Logothetis, 2022; Ningoo et al., 2021).

In line with the need for the detailed elucidation of the TRPC5 modulation profile, this thesis primarily focuses on the functional characterization of phosphorylation sites attributed to the TRPC5 channel through mass spectrometry. Sites selection was based on databases searches complemented with the assessment of structural exposure to the cytoplasm, ensuring accessibility for kinases. We pinpointed four sites of interest and introduced an extra site (Figure 24), that was predicted to be specifically targeted by the ERK1 kinase. ERK1 holds significance due to its activation observed in pathological pain conditions like neuropathic pain and inflammatory responses (Guo & Chen, 2019).

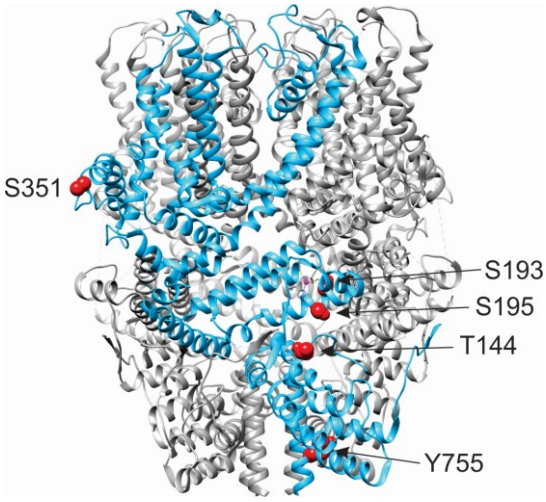

Figure 24: Position of selected phosphorylation sites. *TRPC5 channel structure (PDB ID: 7E4T) with specific residues highlighted as red spheres. These residues are presented on a single subunit, marked in blue for clarity.*

First, phospho-mimicking mutations of TRPC5 at selected sites were constructed using molecular biology methods. For mutants that showed deviations from the control WT in preliminary experiments, phospho-null mutations were subsequently constructed.

Establishing a baseline for the characterization of phospho-mimicking and phosphor-null mutations required an exploration of WT TRPC5 behavior in HEK293T cells, focusing on both voltage-dependent activation and responsiveness to the agonist EA. The previous studies and results obtained in our laboratory demonstrate that non-transfected HEK293T cells exhibit minimal voltage-induced currents not exceeding 500 pA at +200 mV (Samad et al., 2011). Conversely, HEK293T cells transiently transfected with WT hTRPC5 displayed, upon the I/V protocol, outwardly rectifying currents, revealing an average maximum current response of 3.3 ± 0.3 nA at +200 mV. These observations align with findings reported by others (Obukhov et al., 2008) and are consistent with previous study from our laboratory (Zimova et al., 2022). Subsequently, the cells were subjected to a linearly increasing voltage protocol while exposed to 30 nM EA. This elicited a rapid current increase, both at positive and negative membrane potentials. In all measured cells, the first current peak was succeeded by a spontaneous and gradual current decline during the 3-minute EA application and declined to baseline levels during washout with ECS. Key parameters, including amplitude of first EA-induced peak, time of peak and current after 3 minutes of EA exposure were statistically analyzed.

Furthermore, in some cells, the current response tended to oscillate under prolonged exposure to EA, likely due to the effects of Ca^{2+} present in the control ECS at a concentration

of 1 mM. This is not surprising, as prior research has indicated that Ca^{2+} has an impact on agonist-induced gating mechanisms of TRPC5 channels (Blair et al., 2009). It acts from intracellular side as a TRPC5 activator itself and, moreover, triggers cellular pathways that are known to modulate TRPC5 function like PKC-mediated mechanism of desensitization (J. Zhu et al., 2005). Additional experiments would be needed to further elucidate this phenomenon, which would go beyond the scope and aims of this thesis.

The characterization of voltage and agonist-induced responses were done for all five selected putative phosphorylation sites. Distinctive phenotypes were observed for S193 mutations and will be discussed in more detail below. In addition to S193, statistical analysis revealed significant changes in the gating of T144D and S195D mutants.

Mutation of the threonine 144, predicted as an ERK1 target, to aspartate exhibited no changes during EA-induced activation but significantly reduced voltage-induced responses, indicating that T144 may indeed represent a regulatory site that could be of interest for further investigation. While S195D showed voltage-induced responses similar to WT, its time of peak during EA application was 4.5-fold slower, emphasizing the importance of the S193/S195 regulatory site.

The most significant finding of this thesis is the identification of S193 as a crucial regulatory site of the TRPC5 channel. S193 resides in the α helix of the HLH region just above ARD. Interestingly, this helix is in contact with the preceding loop where a zinc-binding site was identified (Song et al., 2021). This loop was unresolved in the first published TRPC5 structures due to low resolution, indicating structural flexibility (Duan et al., 2019). It is possible that such loop may serve as a site of protein-protein or protein-ligand interaction (Papaleo et al., 2016). This area, located intracellularly beneath the cytoplasmic membrane, is exposed to the cytoplasm and appears to be accessible to protein kinases (Figure 24).

In the investigation of the S193A mutation using patch clamp, half of cells exhibited unusually high basal current over -0.5 pA at -80 mV immediately after whole cell configuration formation. At first, it was believed to be caused by a compromised membrane-glass seal or damaged cell membranes. Repeated observations of this phenomenon (acquisition of the S193A data took 10 measurement days instead of the usual 2-3 days for other mutations) suggested constitutive activity associated with S193A. Confirming this was done by a gap-free protocol at the constant voltage of -70 mV, paired with the application of the TRPC5 inhibitor Pico145. The application of Pico145 resulted in a 90% reduction of the S193A basal current.

Examination of voltage-induced gating of the S193 mutations revealed that phosphor-mimicking and phospho-null mutations have opposite effects. Compared to WT channels, the S193A mutation exhibited a significantly higher conductance at both +20 mV and +200 mV, approximately 16-fold and 2.6-fold (respectively) greater than the control WT channels. Conversely, the phospho-mimicking mutation S193D demonstrated a notably lower conductance at +200 mV comparable to non-transfected HEK293T cells.

S193A's heightened activity prevented reliable data acquisition of 3-minute application of EA during the ramp protocol. Meanwhile, experiments with EA have shown that the S193D mutation is functionally expressed. Moreover, S193D mutation exhibited no significant change in the magnitude of responses to EA compared to WT, but notably delayed the time of peak, which was 4-fold slower than WT. The slower kinetics of S193D opening may explain why no measurable currents were observed during I/V protocol, which uses brief 100 ms voltage pulses that are probably too fast to capture S193D activity.

The fact that the magnitude of the EA response both at the peak and at the end of the 3-min EA application is similar to that of WT suggests that the S193D mutation is trafficked to the membrane to the similar extent as WT. On the other hand, the observed heightened activity of S193A may arise from its increased targeting to the plasma membrane.

To compare the cell surface expression of S193A, S193D, and WT channels, we conducted a surface biotinylation assay followed by western blotting. Given historical concerns about the specificity of TRPC5-targeting antibodies among other TRP channels (Franken et al., 2014), we prioritized reliability and high specificity by directing our antibodies towards the GFP-tagged protein which is a well-established methodology in our laboratory. The analysis of the biotinylated surface fractions demonstrated that the quantities of S193A, S193D, and WT TRPC5 ion channels on the cell surface are comparable.

In an effort to explore how S193 phosphorylation affects TRPC5, two molecular simulations were conducted, one for the WT and other for phosphorylated S193. When S193 was phosphorylated, the simulation revealed a substantial 3.6-fold increase in the probability of hydrogen bond formation between S193 and Q309 from an adjacent subunit. In other words, when all four S193 sites within the four subunits of TRPC5 are phosphorylated, it results in a higher occurrence of binding interactions among the subunits through hydrogen bonds formed with Q309.

Considering the heightened activity observed in S193A, it is possible that S193 may be in a partially phosphorylated state in native systems, potentially contributing to the proper functioning of the TRPC5 channel. This effect may be similar to observations with other

already characterized residues S794 and S796 (Sung et al., 2011), where phosphorylation serves to regulate TRPC5 activity through its attenuation.

The limitation of this thesis could be that the selected protocols only focus on two modes of TRPC5 activation. The I/V protocol, applied without a chemical modulator, enables to observe a potential shift in the equilibrium between the open and closed states of the channel upon stimulation by voltage. The use of EA during the voltage ramp protocol captures channel behavior in the presence of a strong chemical activator. However, TRPC5 is modulated by a variety of other stimuli (e.g., PLC pathway or cold), and it is plausible that phosphorylation regulates these other modes, which our measurements did not capture. The reason why no significant changes were observed for some residues tested compared to WT could reside in the protocols chosen, which might have overlooked specific modalities regulated by phosphorylation. Phosphorylated residues often play a role in binding motifs, influencing binding affinity and potentially regulating protein binding with intracellular partners (Menzel et al., 2020). This might be the case for residue the S351, located in the pre-S1 elbow and exposed to the cytoplasm. Pre-S1 elbow has been shown to contribute to the interaction of TRP channels with membrane lipids (Fan et al., 2018; Jin et al., 2017). In this context, the results yielded a sense of disappointment concerning S351, where neither the S351A nor S351D mutations showed any change in the investigated parameters compared to the WT. Despite S351 being ideally positioned to be a regulatory site, predicted as a target of ERK1 and confirmed by mass spectrometry data as a site of phosphorylation.

Another limitation might result from the use of aspartate to mimic phosphorylation. Phospho-mimicking mutation might not always give us the full picture. In the study by (Kozeleková et al., 2022) on the 14-3-3ζ protein, phospho-mimicking mutations did not act exactly like real phosphorylation. The study revealed that the dimerization dissociation constants and oligomeric states differed between the phospho-mimicking mutants and the phosphorylated variant. The phospho-mimicking mutants showed dissimilarities in melting temperatures and hydrophobicity compared to the phosphorylated variant. This suggests that relying solely on these mimicking mutations might not give us the complete understanding of how phosphorylation truly affects proteins. Phosphomimetics are widely used to mimic the phosphorylation effect and are a generally accepted practice in the studies of proteins. However, the results of this thesis should be interpreted with caution, bearing in mind that the mutations only mimic phosphorylation and are not actually phosphorylated.

7 Conclusions

1) Five potential phosphorylation sites, T144, S193, S195, S351 and Y755, were selected utilizing data from mass spectrometry databases and predictive bioinformatics tools.

2) Phospho-mimicking mutations S193D, S195D, T144D, S351D, and Y755D were constructed. Additionally, the phospho-null mutations S193A, S195A, and S351A were prepared based on the preliminary experiments. The products of site-directed mutagenesis were validated using DNA electrophoresis and subsequent sequencing.

3) Wild type TRPC5 channels expressed in HEK293T cells produced outwardly rectifying current responses upon voltage stimulation. The subsequent voltage ramp protocol with EA application elicited persistent channel activity and allowed statistical analysis of the magnitude and the time of the first peak, and the magnitude of the current response after 3 min of EA treatment.

4) A previously unidentified site (S193/S195) at the N-terminus was found to functionally regulate TRPC5. The S193A mutation led to a constitutively active TRPC5 phenotype, whereas the S193D and S195D phospho-mimicking mutations significantly slowed the kinetics of agonist-induced responses.

5) The surface biotinylation assay confirmed that the observed changes in S193A and S193D activity were not due to changes in trafficking of the mutated channels, as both S193D and S193A mutants were present on the membrane in approximately equal amounts as the wild-type TRPC5.

6) Molecular dynamics simulations revealed that S193 phosphorylation leads to an increase in the probability of the hydrogen bond formation with Q309. Higher occurrence of binding interaction among the subunits may explain observed changes in the gating of the S193 mutants.

8 References

Adhya, P., Vaidya, B., & Sharma, S. S. (2023). BTD: A TRPC5 activator ameliorates mechanical allodynia in diabetic peripheral neuropathic rats by modulating TRPC5-CAMKII-ERK pathway. *Neurochemistry International*, *170*, 105609. https://doi.org/10.1016/J.NEUINT.2023.105609

Akbulut, Y., Gaunt, H. J., Muraki, K., Ludlow, M. J., Amer, M. S., Bruns, A., Vasudev, N. S., Radtke, L., Willot, M., Hahn, S., Seitz, T., Ziegler, S., Christmann, M., Beech, D. J., & Waldmann, H. (2015). (-)-Englerin A is a potent and selective activator of TRPC4 and TRPC5 calcium channels. *Angewandte Chemie*, *54*(12), 3787–3791. https://doi.org/10.1002/anie.201411511

Alawi, K. M., Russell, F. A., Aubdool, A. A., Srivastava, S., Riffo-Vasquez, Y., Baldissera, L., Thakore, P., Saleque, N., Fernandes, E. S., Walsh, D. A., & Brain, S. D. (2017). Transient receptor potential canonical 5 (TRPC5) protects against pain and vascular inflammation in arthritis and joint inflammation. *Annals of the Rheumatic Diseases*, *76*(1), 252–260. https://doi.org/10.1136/ANNRHEUMDIS-2015-208886

Albert, A. P., Saleh, S. N., Peppiatt-Wildman, C. M., & Large, W. A. (2007). Multiple activation mechanisms of store-operated TRPC channels in smooth muscle cells. *The Journal of Physiology*, *583*(1), 25–36. https://doi.org/10.1113/JPHYSIOL.2007.137802

Ardito, F., Giuliani, M., Perrone, D., Troiano, G., & Muzio, L. Lo. (2017). The crucial role of protein phosphorylation in cell signalingand its use as targeted therapy (Review). *International Journal of Molecular Medicine*, *40*(2), 271–280. https://doi.org/10.3892/IJMM.2017.3036

Becker, E. B. E., Oliver, P. L., Glitsch, M. D., Banks, G. T., Achillic, F., Hardy, A., Nolan, P. M., Fisher, E. M. C., & Davies, K. E. (2009). A point mutation in TRPC3 causes abnormal Purkinje cell development and cerebellar ataxia in moonwalker mice. *Proceedings of the National Academy of Sciences of the United States of America*, *106*(16), 6706–6711. https://doi.org/10.1073/PNAS.0810599106

Bernal, L., Sotelo-Hitschfeld, P., König, C., Sinica, V., Wyatt, A., Winter, Z., Hein, A., Touska, F., Reinhardt, S., Tragl, A., Kusuda, R., Wartenberg, P., Sclaroff, A., Pfeifer, J. D., Ectors, F., Dahl, A., Freichel, M., Vlachova, V., Brauchi, S., … Zimmermann, K. (2021). Odontoblast TRPC5 channels signal cold pain in teeth. *Science Advances*, *7*(13). https://doi.org/10.1126/SCIADV.ABF5567

Bishnoi, M., & Premkumar, L. S. (2013). Changes in TRP Channels Expression in Painful Conditions. *The Open Pain Journal*, *6*(1), 10–22. https://doi.org/10.2174/1876386301306010010

Blair, N. T., Kaczmarek, J. S., & Clapham, D. E. (2009). Intracellular calcium strongly potentiates agonist-activated TRPC5 channels. *Journal of General Physiology*, *133*(5), 525–546. https://doi.org/10.1085/JGP.200810153

Clapham, D. E. (2003). TRP channels as cellular sensors. *Nature*, *426*(6966), 517–524. https://doi.org/10.1038/nature02196

Cohen, P. (2003). THE STRUCTURE AND REGULATION OF PROTEIN PHOSPHATASES., *58*, 453–508. https://doi.org/10.1146/ANNUREV.BI.58.070189.002321

Duan, J., Li, J., Chen, G. L., Ge, Y., Liu, J., Xie, K., Peng, X., Zhou, W., Zhong, J., Zhang, Y., Xu, J., Xue, C., Liang, B., Zhu, L., Liu, W., Zhang, C., Tian, X. L., Wang, J., Clapham, D. E., Zhang, J. (2019). Cryo-EM structure of TRPC5 at 2.8-Å resolution reveals unique and conserved structural elements essential for channel function. *Science Advances*, *5*(7), 7935–7959. https://doi.org/10.1126/sciadv.aaw7935

Fan, C., Choi, W., Sun, W., Du, J., & Lu, W. (2018). Structure of the human lipid-gated cation channel TRPC3. *ELife*, *7*. https://doi.org/10.7554/eLife.36852

Franken, J., Uvin, P., De Ridder, D., & Voets, T. (2014). TRP channels in lower urinary tract dysfunction. *British Journal of Pharmacology*, *171*(10), 2537. https://doi.org/10.1111/BPH.12502

Gada, K. D., & Logothetis, D. E. (2022). PKC regulation of ion channels: The involvement of PIP2. *Journal of Biological Chemistry*, *298*(6), 102035. https://doi.org/10.1016/J.JBC.2022.102035

Goel, M., Sinkins, W. G., & Schilling, W. P. (2002). Selective association of TRPC channel subunits in rat brain synaptosomes. *Journal of Biological Chemistry*, *277*(50), 48303–48310. https://doi.org/10.1074/JBC.M207882200

Gomis, A., Soriano, S., Belmonte, C., & Viana, F. (2008). Hypoosmotic- and pressure-induced membrane stretch activate TRPC5 channels. *The Journal of Physiology*, *586*(Pt 23), 5633. https://doi.org/10.1113/JPHYSIOL.2008.161257

Guo, W., & Chen, L. (2019). Recent progress in structural studies on canonical TRP ion channels. *Cell Calcium*, *83*, 102075. https://doi.org/10.1016/J.CECA.2019.102075

Guo, W., Tang, Q., Wei, M., Kang, Y., X Wu, J., & Chen, L. (2022). Structural mechanism of human TRPC3 and TRPC6 channel regulation by their intracellular calcium-binding sites. *Neuron*, *110*(6), 1023-1035.e5. https://doi.org/10.1016/J.NEURON.2021.12.023

Hofmann, T., Obukhov, A. G., Schaefer, M., Harteneck, C., Gudermann, T., & Schultz, G. (1999). Direct activation of human TRPC6 and TRPC3 channels by diacylglycerol. *Nature*, *397*(6716), 259–263. https://doi.org/10.1038/16711

Hong, C., Kwak, M., Myeong, J., Ha, K., Wie, J., Jeon, J. H., & So, I. (2015). Extracellular disulfide bridges stabilize TRPC5 dimerization, trafficking, and activity. *Pflugers Archiv European Journal of Physiology*, *467*(4), 703–712. https://doi.org/10.1007/S00424-014-1540-0

Hornberg, J. J., Bruggeman, F. J., Binder, B., Geest, C. R., Bij De Vaate, A. J. M., Lankelma, J., Heinrich, R., & Westerhoff, H. V. (2005). Principles behind the multifarious control of signal transduction. *The FEBS Journal*, *272*(1), 244–258. https://doi.org/10.1111/J.1432-1033.2004.04404.X

Jeon, J. P., Hong, C., Park, E. J., Jeon, J. H., Cho, N. H., Kim, I. G., Choe, H., Muallem, S., Kim, H. J., & So, I. (2012). Selective Galphai subunits as novel direct activators of transient receptor potential canonical (TRPC)4 and TRPC5 channels. *The Journal of Biological Chemistry*, *287*(21), 17029–17039. https://doi.org/10.1074/jbc.M111.326553

Jeong, S. J., Ko, J., Kim, M., Park, K. C., Park, E. Y. J., Kim, J., Baik, Y., Wie, J., Cho, A. E., Jeon, J. H., & So, I. (2019). Englerin A-sensing charged residues for transient receptor potential canonical 5 channel activation. *The Korean Journal of Physiology & Pharmacology*, *23*(3), 191–201. https://doi.org/10.4196/KJPP.2019.23.3.191

Ji, R. R., Baba, H., Brenner, G. J., & Woolf, C. J. (1999). Nociceptive-specific activation of ERK in spinal neurons contributes to pain hypersensitivity. *Nature Neuroscience 1999 2:12*, *2*(12), 1114–1119. https://doi.org/10.1038/16040

Jin, P., Bulkley, D., Guo, Y., Zhang, W., Guo, Z., Huynh, W., Wu, S., Meltzer, S., Cheng, T., Jan, L. Y., Jan, Y. N., & Cheng, Y. (2017). Electron cryo-microscopy structure of the mechanotransduction channel NOMPC. *Nature*, *547*(7661), 118–122. https://doi.org/10.1038/nature22981

Julius, D. (2013). TRP channels and pain. *Annual Review of Cell and Developmental Biology*, *29*, 355–384. https://doi.org/10.1146/annurev-cellbio-101011-155833

Kim, D.-S., Ryu, H. J., Kim, J.-E., & Kang, T.-C. (2013). The Reverse Roles of Transient Receptor Potential Canonical Channel-3 and -6 in Neuronal Death Following Pilocarpine-Induced Status Epilepticus. *Cellular and Molecular Neurobiology*, *33*(1), 99–109. https://doi.org/10.1007/s10571-012-9875-6

Kim, J., Ko, J., Myeong, J., Kwak, M., Hong, C., & So, I. (2019). TRPC1 as a negative regulator for TRPC4 and TRPC5 channels. *Pflugers Archiv European Journal of Physiology*, *471*(8), 1045–1053. https://doi.org/10.1007

Kozeleková, A., Náplavová, A., Brom, T., Gašparik, N., Šimek, J., Houser, J., & Hritz, J. (2022). Phosphorylated and Phosphomimicking Variants May Differ-A Case Study of 14-3-3 Protein. *Frontiers in Chemistry*, *10*. https://doi.org/10.3389/FCHEM.2022.835733

Kuburas, A., Mason, B. N., Hing, B., Wattiez, A. S., Reis, A. S., Sowers, L. P., Loomis, C. M., Garcia-Martinez, L. F., & Russo, A. F. (2021). PACAP Induces Light Aversion in Mice by an Inheritable Mechanism Independent of CGRP. *Journal of Neuroscience*, *41*(21), 4697–4715. https://doi.org/10.1523/JNEUROSCI.2200-20.2021

Leypold, B. G., Yu, C. R., Leinders-Zufall, T., Kim, M. M., Zufall, F., & Axel, R. (2002). Altered sexual and social behaviors in trp2 mutant mice. *Proceedings of the National Academy of Sciences of the United States of America*, *99*(9), 6376–6381. https://doi.org/10.1073/

Li, J., & Stern, D. F. (2005). Regulation of CHK2 by DNA-dependent protein kinase. *Journal of Biological Chemistry*, *280*(12), 12041–12050. https://doi.org/10.1074/jbc.M412445200

Liu, X., Yao, X., & Tsang, S. Y. (2020). Post-Translational Modification and Natural Mutation of TRPC Channels. *Cells*, *9*(1), 135. https://doi.org/10.3390/cells9010135

Lu, R., He, Q., & Wang, J. (2017). TRPC Channels and Alzheimer's Disease. *Advances in Experimental Medicine and Biology*, *976*, 73–83. https://doi.org/10.1007/978-94-024-1088-4_7

Menzel, J., Kownatzki-Danger, D., Tokar, S., Ballone, A., Unthan-Fechner, K., Kilisch, M., Lenz, C., Urlaub, H., Mori, M., Ottmann, C., Shattock, M. J., Lehnart, S. E., & Schwappach, B. (2020). 14-3-3 binding creates a memory of kinase action by stabilizing the modified state of phospholamban. *Science Signaling*, *13*(647), 1436. https://doi.org/10.1126/SCISIGNAL.AAZ1436/

Miyazono, K. ichi, Tabei, N., Morita, S., Ohnishi, Y., Horinouchi, S., & Tanokura, M. (2012). Substrate Recognition Mechanism and Substrate-Dependent Conformational Changes of an ROK Family Glucokinase from Streptomyces griseus. *Journal of Bacteriology*, *194*(3), 607. https://doi.org/10.1128/JB.06173-11

Montell, C., Birnbaumer, L., Flockerzi, V., Bindels, R. J., Bruford, E. A., Caterina, M. J., Clapham, D. E., Harteneck, C., Heller, S., Julius, D., Kojima, I., Mori, Y., Penner, R., Prawitt, D., Scharenberg, A. M., Schultz, G., Shimizu, N., & Zhu, M. X. (2002). A unified nomenclature for the superfamily of TRP cation channels. *Molecular Cell*, *9*(2), 229–231.

Nilius, B., & Owsianik, G. (2010). Transient receptor potential channelopathies. *Pflugers Archiv : European Journal of Physiology*, *460*(2), 437–450. https://doi.org/10.1007/s00424-010-0788-2

Nilius, B., Owsianik, G., Voets, T., & Peters, J. A. (2007). Transient receptor potential cation channels in disease. *Physiological Reviews*, *87*(1), 165–217.

Ningoo, M., Plant, L. D., Greka, A., & Logothetis, D. E. (2021). PIP2 regulation of TRPC5 channel activation and desensitization. *Journal of Biological Chemistry*, *296*. https://doi.org/10.1016/J.JBC.2021.100726

Nishi, H., Shaytan, A., & Panchenko, A. R. (2014). Physicochemical mechanisms of protein regulation by phosphorylation. *Frontiers in Genetics*, *5*(AUG), 97639. https://doi.org/10.3389/FGENE.2014.00270/BIBTEX

Obukhov, A. G., & Nowycky, M. C. (2004). TRPC5 Activation Kinetics Are Modulated by the Scaffolding Protein Ezrin/Radixin/Moesin-Binding Phosphoprotein-50 (EBP50). *JOURNAL OF CELLULAR PHYSIOLOGY*, *201*, 227–235. https://doi.org/10.1002/jcp.20057

Obukhov, A. G., & Nowycky, M. C. (2005). A Cytosolic Residue Mediates Mg2+ Block and Regulates Inward Current Amplitude of a Transient Receptor Potential Channel. *The Journal of Neuroscience*, *25*(5), 1234. https://doi.org/10.1523/JNEUROSCI.4451-04.2005

Okada, T., Inoue, R., Yamazaki, K., Maeda, A., Kurosaki, T., Yamakuni, T., Tanaka, I., Shimizu, S., Ikenaka, K., Imoto, K., & Mori, Y. (1999). Molecular and functional characterization of a novel mouse transient receptor potential protein homologue TRP7. Ca(2+)-permeable cation channel that is constitutively activated and enhanced by stimulation of G protein-coupled receptor. *The Journal of Biological Chemistry*, *274*(39), 27359–27370. https://doi.org/10.1074/jbc.274.39.27359

Okada, T., Shimizu, S., Wakamori, M., Maeda, A., Kurosaki, T., Takada, N., Imoto, K., & Mori, Y. (1998). Molecular cloning and functional characterization of a novel receptor-activated TRP Ca2+ channel from mouse brain. *The Journal of Biological Chemistry*, *273*(17), 10279–10287. https://doi.org/10.1074/jbc.273.17.10279

Ordaz, B., Tang, J., Xiao, R., Salgado, A., Sampieri, A., Zhu, M. X., & Vaca, L. (2005). Calmodulin and Calcium Interplay in the Modulation of TRPC5 Channel Activity: IDENTIFICATION OF A NOVEL C-TERMINAL DOMAIN FOR CALCIUM/CALMODULIN-MEDIATED FACILITATION . *Journal of Biological Chemistry*, *280*(35), 30788–30796. https://doi.org/10.1074/JBC.M504745200

Papaleo, E., Saladino, G., Lambrughi, M., Lindorff-Larsen, K., Gervasio, F. L., & Nussinov, R. (2016). The Role of Protein Loops and Linkers in Conformational Dynamics and Allostery. *Chemical Reviews*, *116*(11), 6391–6423.

Ptakova, A., Mitro, M., Zimova, L., & Vlachova, V. (2022). Cellular context determines primary characteristics of human TRPC5 as a cold-activated channel. *Journal of Cellular Physiology*. https://doi.org/10.1002/JCP.30821

Rubaiy, H. N., Ludlow, M. J., Bon, R. S., & Beech, D. J. (2017). Pico145 - powerful new tool for TRPC1/4/5 channels. *Channels (Austin, Tex.)*, *11*(5), 362–364. https://doi.org/10.1080/19336950.2017.1317485

Sadler, K. E., Moehring, F., Shiers, S. I., Laskowski, L. J., Mikesell, A. R., Plautz, Z. R., Brezinski, A. N., Mecca, C. M., Dussor, G., Price, T. J., McCorvy, J. D., & Stucky, C. L. (2021). Transient receptor potential canonical 5 mediates inflammatory mechanical and spontaneous pain in mice. *Science Translational Medicine*, *13*(595). https://doi.org/10.1126/scitranslmed.abd7702

Samad, A., Sura, L., Benedikt, J., Ettrich, R., Minofar, B., Teisinger, J., & Vlachova, V. (2011). The C-terminal basic residues contribute to the chemical- and voltage-dependent activation of TRPA1. *Biochemical Journal*, *433*(1), 197–204. https://doi.org/10.1042/BJ20101256

Schaefer, M., Plant, T. D., Obukhov, A. G., Hofmann, T., Gudermann, T., & Schultz, G. (2000). Receptor-mediated regulation of the nonselective cation channels TRPC4 and TRPC5. *Journal of Biological Chemistry*, *275*(23), 17517–17526. https://doi.org/10.1074/jbc.275.23.17517

Schwartz, E. S., La, J. H., Scheff, N. N., Davis, B. M., Albers, K. M., & Gebhart, G. F. (2013). TRPV1 and TRPA1 Antagonists Prevent the Transition of Acute to Chronic Inflammation and Pain in Chronic Pancreatitis. *Journal of Neuroscience*, *33*(13), 5603–5611. https://doi.org/10.1523/JNEUROSCI.1806-12.2013

Schwartz, P. A., & Murray, B. W. (2011). Protein kinase biochemistry and drug discovery. *Bioorganic Chemistry*, *39*(5–6), 192–210. https://doi.org/10.1016/J.BIOORG.2011.07.004

Shen, M., Li, L., Li, Y., Gu, X., Bai, L., Xia, C., Xiong, W., & Zuo, Z. (2023). Discovery of potential novel TRPC5 inhibitors by virtual screening and bioassay. *Bioorganic & Medicinal Chemistry*, *94*, 117477. https://doi.org/10.1016/J.BMC.2023.117477

Shi, J., Ju, M., Abramowitz, J., Large, W. A., Birnbaumer, L., & Albert, A. P. (2012). TRPC1 proteins confer PKC and phosphoinositol activation on native heteromeric TRPC1/C5 channels in vascular smooth muscle: comparative study of wild-type and TRPC1-/- mice. *FASEB Journal : Official Publication of the Federation of American Societies for Experimental Biology*, *26*(1), 409–419. https://doi.org/10.1096/fj.11-185611

Song, K., Wei, M., Guo, W., Quan, L., Kang, Y., Wu, J. X., & Chen, L. (2021). Structural basis for human trpc5 channel inhibition by two distinct inhibitors. *ELife*, *10*. https://doi.org/10.7554/ELIFE.63429

Songyang, Z., Lu, K. P., Kwon, Y. T., Tsai, L. H., Filhol, O., Cochet, C., Brickey, D. A., Soderling, T. R., Bartleson, C., Graves, D. J., DeMaggio, A. J., Hoekstra, M. F., Blenis, J., Hunter, T., & Cantley, L. C. (1996). A structural basis for substrate specificities of protein Ser/Thr kinases: primary sequence preference of casein kinases I and II, NIMA, phosphorylase kinase, calmodulin-dependent kinase II, CDK5, and Erk1. *Molecular and Cellular Biology*, *16*(11), 6486–6493

Storch, U., Forst, A. L., Pardatscher, F., Erdogmus, S., Philipp, M., Gregoritza, M., Schnitzler, M. M. Y., & Gudermann, T. (2017). Dynamic NHERF interaction with TRPC4/5 proteins is required for channel gating by diacylglycerol. *Proceedings of the*

National Academy of Sciences of the United States of America, *114*(1), E37–E46. https://doi.org/10.1073/PNAS.1612263114

Storch, U., Forst, A. L., Pardatscher, F., Erdogmus, S., Philipp, M., Gregoritza, M., y Schnitzler, M. M., & Gudermann, T. (2017). Dynamic NHERF interaction with TRPC4/5 proteins is required for channel gating by diacylglycerol. *Proceedings of the National Academy of Sciences of the United States of America*, *114*(1), E37–E46. https://doi.org/10.1073/pnas.1612263114

Strübing, C., Krapivinsky, G., Krapivinsky, L., & Clapham, D. E. (2001). TRPC1 and TRPC5 Form a Novel Cation Channel in Mammalian Brain. *Neuron*, *29*(3), 645–655. https://doi.org/10.1016/S0896-6273(01)00240-9

Sung, T. S., Jeon, J. P., Kim, B. J., Hong, C., Kim, S. Y., Kim, J., Jeon, J. H., Kim, H. J., Suh, C. K., Kim, S. J., & So, I. (2011). Molecular determinants of PKA-dependent inhibition of TRPC5 channel. *American Journal of Physiology. Cell Physiology*, *301*(4), C823-32. https://doi.org/10.1152/ajpcell.00351.2010

Tang, J., Lin, Y., Zhang, Z., Tikunova, S., Birnbaumer, L., & Zhu, M. X. (2001). Identification of common binding sites for calmodulin and inositol 1,4,5-trisphosphate receptors on the carboxyl termini of trp channels. *The Journal of Biological Chemistry*, *276*(24), 21303–21310. https://doi.org/10.1074/jbc.M102316200

Venkatachalam, K., & Montell, C. (2007). TRP channels. *Annual Review of Biochemistry*, *76*, 387–417.

Vinayagam, D., Quentin, D., Yu-Strzelczyk, J., Sitsel, O., Merino, F., Stabrin, M., Hofnagel, O., Yu, M., Ledeboer, M. W., Nagel, G., Malojcic, G., & Raunser, S. (2020). Structural basis of TRPC4 regulation by calmodulin and pharmacological agents. *ELife*, *9*, e60603. https://doi.org/10.7554/eLife.60603

Winn, M. P., Conlon, P. J., Lynn, K. L., Farrington, M. K., Creazzo, T., Hawkins, A. F., Daskalakis, N., Kwan, S. Y., Ebersviller, S., Burchette, J. L., Pericak-Vance, M. A., Howell, D. N., Vance, J. M., & Rosenberg, P. B. (2005). A Mutation in the *TRPC6* Cation Channel Causes Familial Focal Segmental Glomerulosclerosis. *Science*, *308*(5729), 1801–1804. https://doi.org/10.1126/science.1106215

Won, J., Kim, J., Jeong, H., Kim, J., Feng, S., Jeong, B., Kwak, M., Ko, J., Im, W., So, I., & Lee, H. H. (2023). Molecular architecture of the Gαi-bound TRPC5 ion channel. *Nature Communications 2023 14:1*, *14*(1), 1–16. https://doi.org/10.1038/s41467-023-38281-3

Wright, D. J., Simmons, K. J., Johnson, R. M., Beech, D. J., Muench, S. P., & Bon, R. S. (2020). Human TRPC5 structures reveal interaction of a xanthine-based TRPC1/4/5 inhibitor with a conserved lipid binding site. *Communications Biology*, *3*(1), 704. https://doi.org/10.1038/s42003-020-01437-8

Xu, S. Z., Sukumar, P., Zeng, F., Li, J., Jairaman, A., English, A., Naylor, J., Ciurtin, C., Majeed, Y., Milligan, C. J., Bahnasi, Y. M., Al-Shawaf, E., Porter, K. E., Jiang, L. H., Emery, P., Sivaprasadarao, A., & Beech, D. J. (2008). TRPC channel activation by extracellular thioredoxin. *Nature*, *451*(7174), 69–72. https://doi.org/10.1038/nature06414

Yang, Y., Wei, M., & Chen, L. (2022). Structural identification of riluzole-binding site on human TRPC5. *Cell Discovery 2022 8:1*, *8*(1), 1–5. https://doi.org/10.1038/s41421-022-00410-5

Yin, Y., Wu, M., Hsu, A. L., Borschel, W. F., Borgnia, M. J., Lander, G. C., & Lee, S.-Y. (2019). Visualizing structural transitions of ligand-dependent gating of the TRPM2 channel. *Nature Communications*, *10*(1), 3740. https://doi.org/10.1038/s41467-019-11733-5

Yu, K., Wang, Y., Zheng, Y., Liu, Z., Zhang, Q., Wang, S., Zhao, Q., Zhang, X., Li, X., Xu, R. H., & Liu, Z. X. (2023). qPTM: an updated database for PTM dynamics in human, mouse, rat and yeast. *Nucleic Acids Research*, *51*(D1), D479–D487. https://doi.org/10.1093/NAR/GKAC820

Zeng, F., Xu, S. Z., Jackson, P. K., McHugh, D., Kumar, B., Fountain, S. J., & Beech, D. J. (2004). Human TRPC5 channel activated by a multiplicity of signals in a single cell. *The Journal of Physiology*, *559*(Pt 3), 739. https://doi.org/10.1113/JPHYSIOL.2004.065391

Zhang, X., Jin, Q. K., Carr, S. A., & Annan, R. S. (2002). N-Terminal peptide labeling strategy for incorporation of isotopic tags: a method for the determination of site-specific absolute phosphorylation stoichiometry. *Rapid Communications in Mass Spectrometry*, *16*(24), 2325–2332. https://doi.org/10.1002/RCM.864

Zhao, J., Lin King, J. V, Paulsen, C. E., Cheng, Y., & Julius, D. (2020). Irritant-evoked activation and calcium modulation of the TRPA1 receptor. *Nature*, *585*(7823), 141–145. https://doi.org/10.1038/s41586-020-2480-9

Zholos, A. V. (2014). TRPC5. *Handbook of Experimental Pharmacology*, *222*, 129–156. https://doi.org/10.1007/978-3-642-54215-2_6

Zhu, J., Balan, V., Bronisz, A., Balan, K., Sun, H., Leicht, D. T., Luo, Z., Qin, J., Avruch, J., & Tzivion, G. (2005). Identification of Raf-1 S471 as a novel phosphorylation site critical for Raf-1 and B-Raf kinase activities and for MEK binding. *Molecular Biology of the Cell*, *16*(10), 4733–4744. https://doi.org/10.1091/MBC.E05-02-0090/

Zhu, M. H., Chae, M., Kim, H. J., Lee, Y. M., Kim, M. J., Jin, N. G., Yang, D. K., So, I., & Kim, K. W. (2005). Desensitization of canonical transient receptor potential channel 5 by protein kinase C. *American Journal of Physiology - Cell Physiology*, *289*(3 58-3). https://doi.org/10.1152/ajpcell.00440.2004

Zimmermann, K., Lennerz, J. K., Hein, A., Link, A. S., Kaczmarek, J. S., Delling, M., Uysal, S., Pfeifer, J. D., Riccio, A., & Clapham, D. E. (2011). Transient receptor potential cation channel, subfamily C, member 5 (TRPC5) is a cold-transducer in the peripheral nervous system. *Proceedings of the National Academy of Sciences of the United States of America*, *108*(44), 18114–18119. https://doi.org/10.1073/pnas.1115387108

Zimova, L., Ptakova, A., Mitro, M., Krusek, J., & Vlachova, V. (2022). Activity dependent inhibition of TRPC1/4/5 channels by duloxetine involves voltage sensor-like domain. *Biomedicine & Pharmacotherapy*, *152*, 113262. https://doi.org/10.1016/J.BIOPHA.2022.113262

Zimova, L., Sinica, V., Kadkova, A., Vyklicka, L., Zima, V., Barvik, I., & Vlachova, V. (2018). Intracellular cavity of sensor domain controls allosteric gating of TRPA1 channel. *Science Signaling*, *11*(514). https://doi.org/10.1126/scisignal.aan8621